

Czech Technical University in Prague
Faculty of Electrical Engineering
Department of Radioelectronics



Unconventional Techniques for Computational Holography
Nekonvenční techniky pro výpočetní holografii

Arda Özdoğru

Master's Thesis

Master's degree program: Electronics and Communications
Specialization: Audiovisual Technology and Signal Processing
Supervisor: Ing. Karel Fliegel, Ph.D.

Prague, August 2023

Supervisor:

Ing. Karel Fliegel, Ph.D.
Department of Radioelectronics
Faculty of Electrical Engineering
Czech Technical University in Prague
Technická 1902/2, 16627, Prague 6 Czech Republic

Copyright © August 13, 2023 Arda Özdoğru

I. Personal and study details

Student's name: **Ozdogru Arda** Personal ID number: **505361**
Faculty / Institute: **Faculty of Electrical Engineering**
Department / Institute: **Department of Radioelectronics**
Study program: **Electronics and Communications**
Specialisation: **Audiovisual Technology and Signal Processing**

II. Master's thesis details

Master's thesis title in English:

Unconventional Techniques for Computational Holography

Master's thesis title in Czech:

Nekonvenční techniky pro výpočetní holografii

Guidelines:

Provide a state-of-the-art review of digital holography acquisition, processing, and display techniques, including computer-generated holograms. Focus primarily on related optical setups and image processing algorithms for computer-generated hologram encoding and display while also considering unconventional approaches. Implement selected techniques using an experimental laboratory setup or in the form of simulation and evaluate their performance.

Bibliography / sources:

[1] Kostuk, R. K., Holography: Principles and Applications, CRC Press, 2019.
[2] Chang, C., Bang, K., Wetzstein, G., Lee, B., Gao, L., Toward the next-generation VR/AR optics: A review of holographic near-eye displays from a human-centric perspective, Optica, 2020.
[3] Sando, Y., Barada, D., Jackin, B.J., Yatagai, T., Spherical-harmonic-transform-based fast calculation algorithm for spherical computer-generated hologram considering occlusion culling, Applied Optics, 2018.

Name and workplace of master's thesis supervisor:

Ing. Karel Fliegel, Ph.D. Department of Radioelectronics FEE

Name and workplace of second master's thesis supervisor or consultant:

Date of master's thesis assignment: **16.02.2023** Deadline for master's thesis submission: **14.08.2023**

Assignment valid until: **22.09.2024**

Ing. Karel Fliegel, Ph.D.
Supervisor's signature

doc. Ing. Stanislav Vítek, Ph.D.
Head of department's signature

prof. Mgr. Petr Páta, Ph.D.
Dean's signature

III. Assignment receipt

The student acknowledges that the master's thesis is an individual work. The student must produce his thesis without the assistance of others, with the exception of provided consultations. Within the master's thesis, the author must state the names of consultants and include a list of references.

Date of assignment receipt

Student's signature

Declaration

I declare that the presented work was developed independently and that I have listed all sources of information used within it in accordance with the methodical instructions for observing the ethical principles in the preparation of the university thesis.

In Prague, August 13, 2023

.....
Arda Özdoğru

Acknowledgements

First of all, I would like to express my gratitude to my master's thesis supervisor, Ing. Karel Fliegel, Ph.D., for believing in me. He has been a constant source of encouragement and has always been there for me during my times of need of professional guidance. I hope my current and future actions are in the direction to honor you.

I would like to state my appreciation to Ing. František Rund, Ph.D. for helping me during the beginning of my journey and giving me a chance to be a part of the academic environment. This endeavor would not have been possible without him.

I want to express my special thanks to the Dean prof. Mgr. Petr Páta, Ph.D., the department, and the jury of my defense for granting me additional time to complete and conclude my thesis. In return, I have tried to submit a work that is worthy of the education and wisdom that I have received during my time in the master's program.

I want to thank my colleagues and namely Ing. Adam Zizien, for supplying me with the initial know-how, necessary equipment, and software components.

I also want to thank my friends who blessed me with their joy and helped me stay sane.

Finally, I want to share my gratefulness to my family members, for their incredible support and constant belief in me. None of this would have been possible if it wasn't for them. I will always be in their debt.

Abstract

Holography deals with recording and reproducing three dimensional objects using light. It has been developing theoretically since the term was coined in 1948. Computer generated holography is the field that processes and reconstructs computationally recorded holograms. With the advancements in computational power and manufacturing technology in the recent years, many new methods for processing and visually reconstructing holograms have been published.

This work focuses on encoding and displaying technologies for holograms. The focus is especially put on spherical computer generated holography and light field displays.

A spherical harmonics transform based calculation method for spherical computer generated holography is investigated. A software, capable of converting publicly maintained holographic images to light field images and displaying them in a light field display, is developed. Based on these, a workflow to encode, manipulate, and display object holograms is drafted.

Spherical harmonics transform based method seems promising however further research is necessary to be able to create a commercial system, drafted workflow supplies an approximate guide. The software can be expanded to cover all available holographic image datasets and light field displays. The road map for future research and development is identified.

Keywords: spherical harmonics transform, spherical computer generated holography, light field display, holographic image, light field image, conversion, image processing.

Abstrakt

Holografie se zabývá záznamem a reprodukcí trojrozměrných objektů pomocí světla. Teoreticky se vyvíjí od roku 1948, kdy byl tento termín zaveden. Počítačová holografie je obor, který zpracovává a rekonstruuje počítačově zaznamenané hologramy. S rozvojem výpočetního výkonu a výrobních technologií v posledních letech bylo publikováno mnoho nových metod zpracování a vizuální rekonstrukce hologramů.

Tato práce se zaměřuje na technologie kódování a zobrazování hologramů. Důraz je kladen zejména na sférickou počítačem generovanou holografii a zobrazení světelného pole.

Je zkoumána metoda výpočtu sférické harmonické transformace založená na sférickou počítačem generovanou holografii. Je vyvinut software, který je schopen převádět veřejně udržované holografické obrazy na obrazy světelného pole a zobrazovat je na displeji světelného pole. Na jejich základě je navržen pracovní postup pro kódování, manipulaci a zobrazení hologramů objektů.

Metoda založená na sférické harmonické transformaci se zdá být slibná, nicméně je nutný další výzkum, aby bylo možné vytvořit možné vytvořit komerční systém. V práci je představen rámcový postup. Software lze rozšířit tak, aby pokrýval všechny dostupné sady holografických obrazových dat a zobrazení světelného pole. Jsou prezentovány náměty na navazující výzkum.

Klov slova:

sférická harmonická transformace, sférická počítačem generovaná holografie, zobrazení světelného pole, holografický obraz, obraz světelného pole, konverze, zpracování obrazu.

Contents

Declaration	v
Acknowledgements	vii
Abstract	ix
Abstrakt	xi
Abbreviations	xvii
1 Introduction	1
2 Background on Holography and Light	3
2.1 Theoretical background of light	3
2.1.1 Electromagnetic waves	4
2.1.2 Polarization of light	6
2.1.3 Coherence	7
2.1.4 Diffraction	8
2.1.5 Effect of lenses	9
2.2 Holograms	10
2.2.1 Computer generated holography (CGH)	12
2.2.2 Digital holography (DH)	14
2.3 Spherical harmonics and application of higher order ambisonics	16
3 State-of-the-Art	19
3.1 Methods of computer generated holography	19
3.2 Display technology and volumetric displays	24
3.2.1 SeeReal Technologies and holographic displays	25
3.2.2 QinetiQ and the Active Tiling system	26
3.2.3 HoloVizio	27

3.3	Light field display technology	27
3.3.1	Plenoptic function	27
3.3.2	Technical explanation	28
3.3.3	Possible usage of LFDs	29
3.3.4	Looking Glass Portrait	29
3.4	JPEG Pleno database	30
3.4.1	Datasets for holography	31
3.5	JPEG Pleno numerical reconstruction software for holograms	31
3.6	Light field and holography correlation and conversion	32
4	A Method to Encode and Display Holograms	35
4.1	Introduction to the method	35
4.2	Encoding of object wavefields based on SHT	38
4.2.1	Reasoning of selection of the encoding method	38
4.2.2	Wavefront on the spherical surface	40
4.2.3	Sampling pitch	42
4.2.4	Practical trial of SHT encoding	43
4.3	Displaying of holographic images on LFD	44
4.3.1	Input Selection and Limitations	45
4.3.2	An example of conversion using Hol2LFD	48
5	Conclusions	53
5.1	Summary	53
5.2	Contributions of the master's thesis	55
5.3	Future work	56
6	Appendix	57
	Bibliography	59

List of Figures

2.1	Levels of optics scale on each other.	3
2.2	Polarization of light. Top left: parallel, top right: perpendicular, bottom left: circular, bottom right: elliptical polarization.	7
2.3	Coherent plane wave wavefronts where the propagation of direction is to the right.	7
2.4	Huygen-Fresnel Diffraction illustration (taken from [2])	8
2.5	4f optical system resulting in the Fourier transformed image (taken from [2]).	10
2.6	Basic holography steps. a) create the interference pattern, b) record the pattern through a holographic material, c) using the same reference beam, or d) using the conjugate of the reference beam to recreate the image (taken from [2]).	11
2.7	Inline hologram (taken from [2]).	11
2.8	Recording and reconstructing Bragg circle for different wavelength (taken from [2]).	13
2.9	a) Obtaining and d) reconstruction of optical holography, c) obtaining and e) reconstruction of computer generated holography (CGH), c) obtaining and f) reconstruction of digital holography (DH) (taken from [14]). The frames with PC mean that part is calculated in the computer.	15
2.10	Spatial representation of spherical harmonics of order n degree m (taken from [9]).	17
3.1	Light fields of different scenery are encoded with spherical harmonics. The directional curves indicate the direction that the panoramic images are enlightened from (taken from [26]).	20
3.2	System illustration built within the research presented in [22]. L: lens; BS: beamsplitter; F: optical filter; M: mirror; C: collimator. The colors are for ray tracing (taken from [22]).	21
3.3	Figures (a and b) depict the propagation model between a plane and a sphere, while figures (c and d) show the schematic of SCGH generation using the phase compensation (PC) method (taken from [27]).	22

3.4	Reconstructed images are given. (a), (b), and (c) represent the reconstructed images there are at different depths, respectively at $z = -2.5$ mm, 0 mm, and 2.5 mm (taken from [28]).	23
3.5	Schematic diagram for (a) object-image-plan and (b) image-object-plane methods (taken from [29]).	24
3.6	Correspondence between light and processing methods (taken from [29]).	25
3.7	Calculation times required under the various conditions, N_O, N_Θ, N_Φ , and N_P represent sampling numbers of the object space, Θ, Φ , and the number of point light sources constituting the 3D object, respectively (taken from [30]).	26
3.8	LFD layer by layer decomposition illustrating the working principle (taken from [59]).	28
3.9	Generic lenticular lens array (taken from [60]).	30
3.10	Holographic image data that is contained in ballet8k4k frame 22 holographic image in BCOM dataset. On the left real part of the hologram and on the left the imaginary part of the hologram is represented.	32
3.11	JPEG Pleno numerical reconstruction software for holography workflow (taken from [61]).	33
4.1	Block diagram of the proposed method. The method is divided into two parts. On the left of the dashed line, the encoding of the objects is shown and on the right of the dashed line, the displaying of the holograms is shown. The external inputs to the system are given in green color, the intermediate steps are given in turquoise color, and the outputs of the system are given in orange color. The yellow-colored box indicates the implemented system Hol2LFD.	36
4.2	Equidistant laser distribution on a spherical and hemispherical surface, the tiling structure is also illustrated on the spherical surface.	37
4.3	SHT encoding block diagram.	39
4.4	(a) Selection of components on the hemispherical surface of radius $1/\lambda$, (b) observation vector a and Fourier component points vector b where (u, v, w) is practically equivalent to cartesian coordinates (x, y, z) in spatial frequency domain. Ω represents the angle between vectors \vec{a} and \vec{b} (taken from [30]).	41
4.5	Encoded and decoded O_s	43
4.6	Block diagram of the displaying method. The external inputs to the system are given in green color, the intermediate steps are given in turquoise color, and the outputs of the system are given in orange color. The whole system constitutes the Hol2LFD.	44
4.7	Synthetic aperture illustration (taken from [61]).	45
4.8	Synthetic aperture on Fourier components determines which parts will be propagated. Here θ , on the left, represents the horizontal rotation angle, and ψ , on the right, represents the aperture size (taken from [74]).	46

LIST OF FIGURES

4.9	Holographic image data that is contained in dices4k holographic image in BCOM dataset. On the left real part of the hologram and on the left imaginary part of the hologram is represented. The reconstructed version of this image is in Fig. 4.11	47
4.10	Input page of Hol2LFD, the necessary input parameters are entered for dices4k quilt image construction.	48
4.11	Single rendering (propagation by NRSH) of dices4k of BCOM dataset, with reconstruction parameters: -7.23404 degrees horizontal rotation, 6 degrees aperture size, and 0.0017 meters of reconstruction distance.	49
4.12	Quilt image ready to be sent to LFD that was reconstructed with input parameters to Hol2LFD: -20 to 20 degrees horizontal rotation, 6 vertical and 8 horizontal images, 6 degrees aperture size, and 0.0017 meters of reconstruction distance.	50
4.13	LGP displaying processed dices4k of BCOM dataset from 3 different angles. .	51

Abbreviations

Miscellaneous Abbreviations

3D	Three dimensional
DH	Digital holography
CGH	Computer generated holography
SLM	Spatial light modulators
LFD	Light field display
SHT	Spherical harmonics transform
BW	Bandwidth
BDCE	Binary detour phase encoding
BI-CGH	Binary interferogram computer generated holograms
BFT	Binary Fourier transform hologram
IPR	Iterative phase retrieval
HPC	Holographic phase conjugation
PC	Personal computer
CCD	Charge-coupled device
CMOS	Complementary metal-oxide-semiconductor
DHI	Digital holographic interferometry
DHM	Digital holographic microscopy
DHSD	Digital holographic stereo display (
NDT	Non-destructive testing
SCGH	Spherical computer generated holography
HOA	Higher order ambisonics
ACN	Ambisonics channel numbering
FFT	Fast Fourier transform
WRP	Wavefront recording plane
PS	Point source
OIP	Object-image-plane
IOP	Image-object-plane

ABBREVIATIONS

HOLF	Horizontal optical path filter
PSF	Point spread function
DNN	Deep Neural Network
MDHGN	Multi-depth hologram generation network
2D	Two dimensional
EASLM	Electrically addressed spatial light modulator
OASLM	Optically addressed spatial light modulator
FLCoS	Ferroelectric crystal on silicon
LGP	Looking Glass Portrait
JPEG	Joint Photographic Experts Group
NRSH	Numerical reconstruction software for holograms
FOV	Field of view
3D FFT	three dimensional fast Fourier transform
2D FFT	two dimensional fast Fourier transform
GUI	Graphical user interface
V:H	Vertical:Horizontal
API	Application programming interface

Introduction

Light is one of the most fundamental sources of life and energy in the world.

Holography is a branch of optics that deals with the recording and reproduction of three-dimensional (3D) images, which was coined by Dennis Gabor in 1948, [1]. It involves the interference of light from a reference beam and an object beam to produce a hologram that encodes the 3D information of the object. The hologram, when illuminated by a similar reference beam, produces a virtual image of the object that appears to be floating in space. This makes holography a promising technology for a variety of applications, including 3D displays, security, and medical imaging.

In recent years, the development of digital holography (DH) and computer generated holography (CGH) has revolutionized the field of holography. Digital holography involves the acquisition, processing, and reproduction of holograms using digital technologies, whereas CGH involves the generation of holograms using computer algorithms. Both digital holography and CGH offer several advantages over traditional holography, including the ability to manipulate and modify the holograms after they are recorded, and the ability to generate holograms of virtual objects that do not exist in the physical world. Especially after spatial light modulators (SLM) are developed, the research and application of dynamic CGH are advanced quickly. However, despite these advances, there are still several challenges associated with the acquisition, processing, and reproduction of digital holograms. For example, the quality of the holograms can be affected by noise, aberrations, and other artifacts introduced during the image acquisition process. Similarly, the processing and reproduction of digital holograms can be computationally intensive and may result in artifacts or loss of information.

A more important challenge can be shown as the accurate and easy encoding (sampling and representation) of complex objects and their dynamic 360-degree reconstruction in a bounding frame-free environment through fast calculation. Accompanied by that challenge is the proper physical display system which would enable such a reproduction.

In this report, after the state-of-the-art CGH is reviewed, a possible encoding and reproduction approach for 360 bounding frame-free CGHs based on the utilization of spherical harmonics is tried to be drafted. In order to establish, a complete work flow that also

consists of displaying, a software was constructed to enable holographic image to light field display (LFD) image conversion and displaying of the processed images are established. In other words, a complete method to encode object holograms and to display these holograms is tried to be established. The working principle of every used method is explained in their related sections. The software is publicly shared to enable further researches and enthusiast to work on and develop the workflow.

This work is arranged in such a way that, in chapter 2, the theoretical background for light waves, holograms, CGH, and DH is given along with a brief explanation of a mathematical description of spherical harmonics transform (SHT). In chapter 3, the state-of-the-art in the areas of hologram generation, CGH, DH, and display technologies are briefly described. In chapter 4, the proposed method and the experimental work are presented. Lastly, in chapter 5, this work is summarized, contributions are highlighted, and future work is described.

Background on Holography and Light

In this chapter, the background knowledge for understanding the implemented work is given. The fundamental mathematical and conceptual knowledge of light theory, holography, and spherical harmonics is presented from the ground up.

2.1 Theoretical background of light

This chapter aims to provide a brief review of the electromagnetic principles of light that are necessary to understand holography. Optics is a wide field of physics and has been researched for a long time. The properties of light and its interactions are understood deeply. A rough division of conceptual understanding of light can be seen in Fig. 2.1. Starting from Maxwell, the electromagnetic properties of light are understood. Here, only the theoretical part of electromagnetic optics is explained and subtopics are omitted.

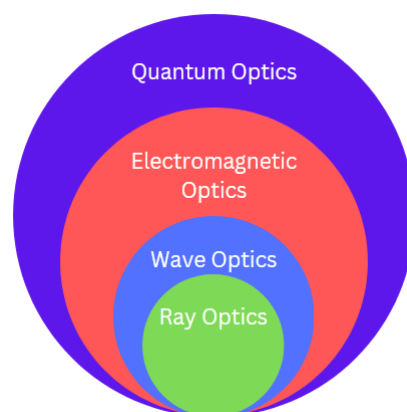


Figure 2.1: Levels of optics scale on each other.

2.1.1 Electromagnetic waves

Electromagnetic waves reveal themselves in nature in many ways. From incredibly small wavelengths of gamma rays to extremely low-frequency radio waves, the electromagnetic spectrum is highly utilized in many areas such as communications technology, astronomy, electronics, medicine, nuclear technology, and holography. Visible light constructs a tiny portion of the electromagnetic spectrum. How the electromagnetic waves behave and the propagation of light is fully defined by Maxwell equations which are as follows:

$$\nabla \cdot \vec{E} = \frac{\rho}{\epsilon_0}, \quad (2.1)$$

$$\nabla \cdot \vec{B} = 0, \quad (2.2)$$

$$\nabla \times \vec{E} = -\frac{\partial \vec{B}}{\partial t}, \quad (2.3)$$

$$\nabla \times \vec{B} = \mu_0 \vec{J} + \mu_0 \epsilon_0 \frac{\partial \vec{E}}{\partial t}, \quad (2.4)$$

where \vec{E} is the electric field, \vec{B} is the magnetic field, ρ is the charge density, ϵ_0 is the electric constant, μ_0 is the magnetic constant and \vec{J} is the current density. The ∇ denotes $\nabla = \frac{\partial}{\partial x} + \frac{\partial}{\partial y} + \frac{\partial}{\partial z}$. The fields can be converted to each other in such a way:

$$\vec{D} = \epsilon_0 \vec{E} \quad (2.5)$$

$$\vec{B} = \mu_0 \vec{H} \quad (2.6)$$

$$\vec{J} = \sigma \vec{E} \quad (2.7)$$

where \vec{B} is the magnetic field, \vec{D} is the electric flux density, ϵ is the permittivity, μ is the permeability, and σ is the conductivity of the material in which the fields exist. The permittivity and the permeability of the medium can be calculated as follows:

$$\epsilon = \epsilon_r \epsilon_0 \quad (2.8)$$

$$\epsilon_0 = 8.854 \times 10^{-12} \text{Farads/m}$$

$$\mu = \mu_r \mu_0 \quad (2.9)$$

$$\epsilon_0 = 4\pi \times 10^{-7} \text{Henry/m}$$

where ϵ_r is the relative permittivity, and ϵ_0 is the free-space or vacuum permittivity. Similarly, μ_r is the relative permeability and μ_0 is the free-space permeability of the material.

In most optic elements, there are no free charges of currents hence Maxwell's equations become,

$$\nabla \times \vec{E} = -\frac{\partial \vec{B}}{\partial t} \quad (2.10)$$

$$\nabla \times \vec{H} = \frac{\partial \vec{D}}{\partial t} \quad (2.11)$$

$$\nabla \cdot \vec{E} = 0 \quad (2.12)$$

$$\nabla \cdot \vec{B} = 0 \quad (2.13)$$

$$\vec{D} = \epsilon \vec{E} \quad (2.14)$$

$$\vec{H} = \frac{\vec{B}}{\mu_0} \quad (2.15)$$

By substituting \vec{D} and \vec{H} into the two equations above we get the wave equation for the electric field in the form:

$$\nabla^2 \vec{E} - \frac{n^2}{c_0^2} \frac{\partial^2 \vec{E}}{\partial t^2} = 0 \quad (2.16)$$

$$c_0^2 = \frac{1}{\epsilon_0 \mu_0} \quad (2.17)$$

where c_0 is the speed of light in vacuum and n is the refractive index of the medium. In different mediums the interaction of light with the medium changes because of the refractive index of that medium. Hence, $c = c_0/n$ is the speed of the light in that medium.

The wave equation for the electric field is derived from Maxwell's equations in the absence of charges and currents for isotropic, homogeneous, and non-dispersive media. Such media can be described as ideal media in terms of supplying uniformity in the physical domain, creating a uniform refractive index throughout the light spectrum and volume of the medium, and immunity from the direction of propagation and polarization. Although ideal mediums are not existent, for the sake of simple propagation of electric field through space and time Eq. 2.17 holds correctness. A similar result can be driven for the magnetic field which is orthogonal to the electric field:

$$\vec{E} \cdot \vec{H} = 0, \quad (2.18)$$

and direction of propagation is given by the Poynting vector:

$$\vec{S} = \vec{E} \times \vec{H} \quad (2.19)$$

The propagation vector (also known as wave vector or wave number) is a vector that describes the direction and magnitude of the propagation of an electromagnetic wave. The propagation vector is given by the symbol k and it is defined as:

$$k = \frac{\omega}{c} \hat{n} \quad (2.20)$$

2. BACKGROUND ON HOLOGRAPHY AND LIGHT

where $\omega = \frac{2\pi}{\lambda}$ is the angular frequency of the wave, c is the speed of light in a vacuum and $\hat{\mathbf{n}}$ is a unit vector that represents the direction of propagation of the wave. In 3 dimensions, propagation vector can be written as $k = k_x\hat{x} + k_y\hat{y} + k_z\hat{z}$ and can be calculated as:

$$k_x = \frac{2\pi n}{\lambda}\cos\alpha, k_y = \frac{2\pi n}{\lambda}\cos\beta, k_z = \frac{2\pi n}{\lambda}\cos\gamma \quad (2.21)$$

where α, β, γ are the angle that the propagation vector k makes with the relative axis.

Non-trivial solution of the wave equation in Eq. 2.17 in cartesian coordinates is

$$\vec{E}(x, y, z, t) = E_0\hat{u}(\vec{k} \cdot \vec{r} - \omega t + \phi) \quad (2.22)$$

where E_0 is the amplitude, \hat{u} is the unit vector of direction, \vec{r} is the distance vector from the point of origin and ϕ is the phase as a function of position. When Eq. 2.22 expressed in complex representation and the physical (real) part of the field is taken and used in time independent wave equation which is called as Helmholtz equation [3].

$$\nabla^2 E + k^2 E = 0 \quad (2.23)$$

The resulting electric field is:

$$E(x, y, z) = E_0 e^{j(\vec{k} \cdot \vec{r} - \phi)} \quad (2.24)$$

A similar result is derived for the magnetic field as well.

2.1.2 Polarization of light

Polarization is an important property of electromagnetic waves. It mainly describes the oscillation plane of \vec{E} and mainly in 3 categories as follows:

1. **Linear:** \vec{E} oscillates in a single plane and is further noted as parallel and perpendicular based on its interaction with the optical element.
2. **Circular:** \vec{E} oscillates in 2 planes meaning that it contains equal magnitudes of components in two dimensions

$$\vec{E}(z, t) = \vec{E}_x + \vec{E}_y = E_0\hat{x}\cos(kz - \omega t) + E_0\hat{y}\sin(kz - \omega t) \quad (2.25)$$

which creates a rotation of the electrical field around the propagation axis z . That rotation can be clockwise or anti-clockwise

3. **Elliptical:** This is similar to circular polarization except the $E_{x0} \neq E_{y0}$ and they contain a phase difference in between.

These types of polarization are illustrated in 2.2. For our case, linear polarization is going to be used. For further explanation, [4] can be referred to for a detailed explanation.

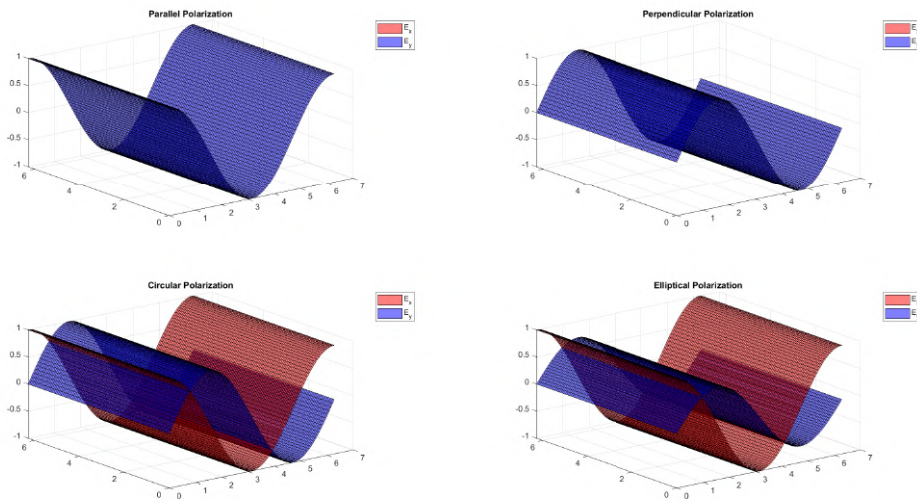


Figure 2.2: Polarization of light. Top left: parallel, top right: perpendicular, bottom left: circular, bottom right: elliptical polarization.

2.1.3 Coherence

Coherence carries an important role in holography. It can be characterized as *temporal coherence* and *spatial coherence* both of which are of high importance. An illustration of a plane wave that exhibits temporal and spatial coherence is in Fig. 2.3.

Temporal coherence: Temporal coherence states that the phase difference between two different points of the field stays the same throughout time or distance in the direction

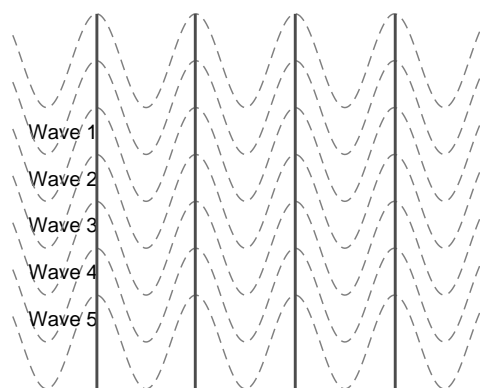


Figure 2.3: Coherent plane wave wavefronts where the propagation of direction is to the right.

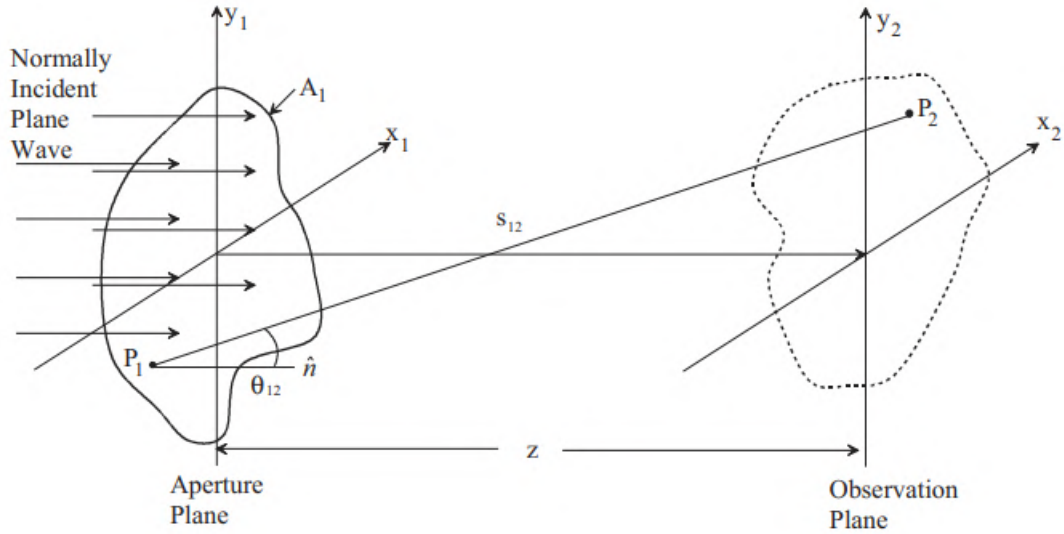


Figure 2.4: Huygen-Fresnel Diffraction illustration (taken from [2])

of propagation. Meaning all wavefronts in Fig. 2.3 are the same.

Spatial coherence: Spatial coherence states that all the electrical fields that construct a wavefront have the same properties. For purely monochromatic sources, this is automatically satisfied because of the absence of dispersion caused by the wavelength dependence of the refractive index of the medium. However, because of physical limitations, it is hard to generate a single-wavelength light source. The line function nature of even laser sources (known as the most coherent light sources) will be preserved. Laser sources in recent research show around 5 nm bandwidth (BW), see [5].

2.1.4 Diffraction

When the optical field passes through objects it interacts which changes the spatial properties of the field. This can be explained by diffraction. Here, some ideas are tried to briefly be explained, for a detailed explanation please refer to [6].

1. **Huygen-Fresnel diffraction:** Each point in a wavefront acts as a spherical point source and the overlapping points create the next wavefront, see Fig. 2.4. Then the field at point 2 originating from point 1 can be calculated as:

$$E(x_2, y_2) = \frac{1}{j\lambda z} \iint_{A_1} E(x_1, y_1) e^{jks_{12}} dx_1 dy_1 \quad (2.26)$$

where s_{12} is the path between two points and z is the projection of that distance along the direction of propagation. This gives rise to simplifications to the Eq. 2.26 based on the *nearness* (Fresnel) or *farness of field* (Fraunhofer) of observation.

2. **Fresnel diffraction:** Essentially, if s_{12} is sufficiently close to the optical axis at the point of observation the Fourier transform of the electric field with a changing quadratic phase function is observed.
3. **Fraunhofer diffraction:** For far fields, and small angles of θ in Fig. 2.4, the field is the exact Fourier transform of the initial field without any phase dependence on the distance z .

$$E(x_2, y_2) = \frac{e^{jkz} e^{j\frac{k}{z}(x_2^2 + y_2^2)}}{j\lambda z} \iint E(x_1, y_1) e^{-j2\pi(v_x x_1 + v_y y_1)} dx_1 dy_1 \quad (2.27)$$

where

$$v_x = \frac{x_2}{\lambda z}; v_y = \frac{y_2}{\lambda z} \quad (2.28)$$

However, the far-field assumption requires that,

$$\frac{k}{2z}(x_1^2 + y_1^2) = \frac{\pi}{\lambda z}(x_1^2 + y_1^2)_{max} \ll 1, \quad (2.29)$$

which results in a distance required for $\lambda = 500nm \Rightarrow z = 600m$. However, the lenses can create this through the utilization of focal points as in Fig. 2.5.

2.1.5 Effect of lenses

Lenses are essentially objects that interact with light. Their transmittance function directly affects the electric field as such,

$$E_{out}(x, y) = t_{lens}(x, y) E_{in}(x, y) \quad (2.30)$$

$$t_{lens}(x, y) = e^{-j\phi(x, y)} \quad (2.31)$$

$$\phi(x, y) = -\frac{2\pi}{\lambda} \frac{x^2 + y^2}{2f} \quad (2.32)$$

where ϕ is the spatially varying phase function of the lens. When this lens is coupled with an object placed in the focal plane, the far field effect is created and the resulting Fourier transform of the object field at the other focal plane. A good illustration is given in [2] shown in Fig 2.5. For example a square aperture at the point of object in Fig. 2.5 will result in a 2D sinc function at the front focal plane of L1.

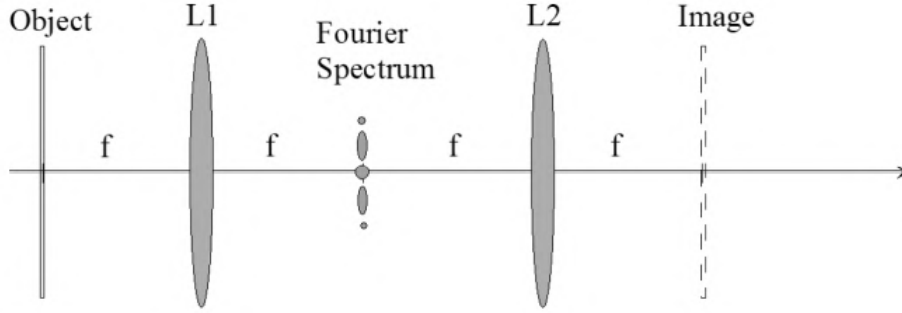


Figure 2.5: 4f optical system resulting in the Fourier transformed image (taken from [2]).

2.2 Holograms

In this section, the general principle for hologram forming is introduced. Although holograms are a complicated and a vast topic, only the chosen parts that are converging with our approach are explained. For a more complete and detailed explanation of the principles of holograms please refer to [2].

For coherent beams when the beam is split and one of the beams are shine upon an object, the wavefronts of the beam take the shape of the object. The beams are expressed as:

$$\tilde{r} = a_r e^{[j(\vec{k}_r \vec{r} + \phi_r(x,y,z))]} \quad (2.33)$$

$$\tilde{o} = a_o e^{[j(\vec{k}_o \vec{r} + \phi_o(x,y,z))]} \quad (2.34)$$

where a are the amplitudes of the waves, \vec{k} are the propagation vectors, \vec{r} are the position vector and ϕ are the phases of the waves.

Later when the object wave is crossed with the reference beam the forming interference pattern can be recorded in a holographic material which then can be used to regenerate the holographic image 2.6. The intensity of the interference pattern can be found as:

$$I = |\tilde{r} + \tilde{o}|^2 \quad (2.35)$$

$$= |\tilde{r}|^2 + |\tilde{o}|^2 + \tilde{r}\tilde{o}^* + \tilde{o}\tilde{r}^* \quad (2.36)$$

$$= a_r^2 + a_o^2 + 2a_o a_r \cos[(\vec{k}_r - \vec{k}_o)\vec{r} + \phi_d] \quad (2.37)$$

hence the intensity is a function of position and the phase difference (ϕ_d) between the object and reference beams.

Types of holograms can be briefly explained as follows:

1. Reflection hologram: A reflection hologram is a hologram that is viewed by reflecting light off its surface. This type of hologram is used primarily as a security feature on credit cards, passports, and other identification documents.

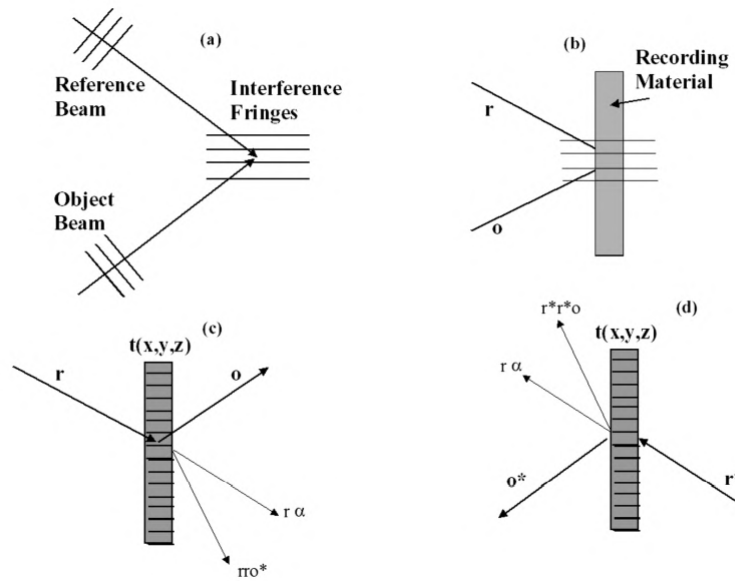


Figure 2.6: Basic holography steps. a) create the interference pattern, b) record the pattern through a holographic material, c) using the same reference beam, or d) using the conjugate of the reference beam to recreate the image (taken from [2]).

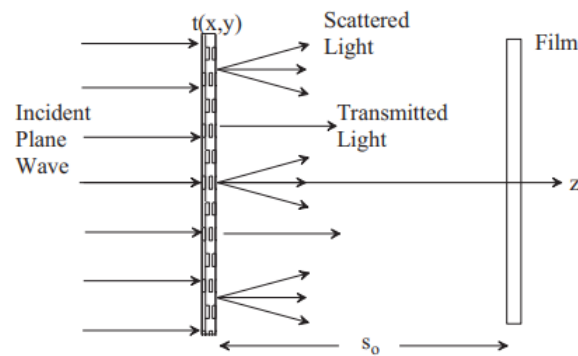


Figure 2.7: Inline hologram (taken from [2]).

2. Transmission hologram: A transmission hologram is a hologram that is viewed by shining light through it. This type of hologram is used in the display of holographic images and is often used in advertising and trade shows.

In terms of hologram geometries, there are several different types, including:

1. In-line hologram: In-line holograms are created when the reference and object beams are aligned in the same direction. This type of hologram provides a clearer image

however the reference beam decreases the contrast of the hologram as it creates background noise. Moreover, it creates a duplicate (conjugate) image. In Fig. 2.7, geometry is given.

2. Off-axis hologram: Off-axis holograms are created when the reference and object beams are not aligned. This type of hologram provides a more complex image that is harder to realize. The schematic is as in Fig. 2.7, but the reference beam is not supplied through the transmittance object, instead supplied with an angle directly to the film.
3. Fourier hologram: Fourier holograms are created using a mathematical algorithm that transforms the object wave into its Fourier components. This type of hologram provides a high-resolution image but is also more difficult to produce and uses geometry as in Fig. 2.5.
4. Fraunhofer hologram: Fraunhofer holograms are created using the Fraunhofer diffraction theory, which states that the image of an object is proportional to its Fourier transform. This type of hologram provides a clear image with good depth information but is limited by the size of the object being imaged.

Each type of hologram has its own unique characteristics which create certain limitations and aberrations during the regeneration. For detailed explanations refer to section 3.4 and section 3.5 of [2].

Grating vector \vec{K} , is also another important parameter of holography. It indicates the frequency and the direction of interference fringes in the recording material that would later be used to reconstruct the hologram.

In case of a mismatch of the wavelength of construction and reconstruction the Bragg circle can be followed as in Fig. 2.8.

where k_{11}, k_{12} are the construction propagation vectors, k_{21}, k_{22} are the reconstruction vectors. Vectors k'_{21}, k'_{22} are not important for our case. The grating vector is the vector difference and

$$\vec{K} = k_{11} - k_{12} \quad (2.38)$$

$$|\vec{K}| = \frac{2\pi}{\Lambda} \quad (2.39)$$

where Λ is the distance between fringes that are set fixed during recording. In the reconstruction, a different wavelength can be used to recreate the image. However, in such a case the reconstruction propagation vectors should be calculated with respect to Bragg circle in Fig. 2.8.

2.2.1 Computer generated holography (CGH)

Analog holography requires the physical generation of the object and reference beams, which is not practical, especially for dynamic applications. However, with recent advancements in optical elements, the wavefront of a coherent laser beam can be controlled by

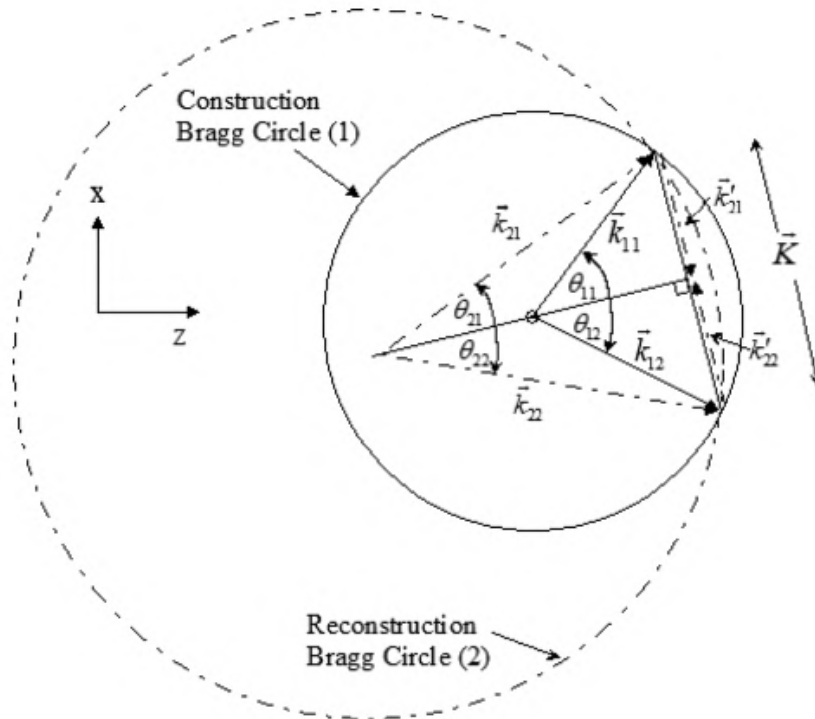


Figure 2.8: Recording and reconstructing Bragg circle for different wavelength (taken from [2]).

a spatial light modulator (SLM) which allows dynamic manipulation of the wavefront [2, 12, 13].

Each element between the light source and the final holographic image can be considered an optical transfer (transmittance) function that is spatially manipulating the wavefront, and the directional \vec{k} of the beam. Such elements include pinholes, lenses, propagation through the medium, wavelength mismatch between recording and recreation waves and etc.

For a desired image at a desired position, the transfer functions can be traced back to the point of wavefront generation. Hence, the desired object field can be designed in the computer and the aberrations can be incorporated during the object field generation. Later, this modified object wave can be generated by an electronically controllable SLM.

There are various types of encoding methods for CGH some are explained briefly as:

1. Binary detour phase encoding (BDCE): This method involves encoding binary phase information into the hologram by creating a detour phase pattern that represents the object. The detour phase pattern is created by modifying the phase of the reference wave in a specific way, such that the resulting interference pattern forms the desired binary phase pattern. The resulting hologram can be easily implemented using binary

optical elements, such as a binary phase-only filter [2].

2. Binary interferogram computer generated holograms (BI-CGH): This method involves encoding binary phase information into the hologram by creating a binary interferogram. The binary interferogram is formed by superimposing a binary phase object with a reference wave, such that the resulting interference pattern forms the desired binary phase pattern. The resulting hologram can be easily implemented using binary optical elements, such as a binary phase-only filter [2].
3. Binary Fourier transform hologram (BFT): This method involves encoding binary phase information into the hologram by creating a binary Fourier transform hologram. The binary Fourier transform hologram is formed by computing the Fourier transform of the binary phase object and multiplying the resulting diffraction pattern by a binary phase mask. The binary phase mask is used to control the diffraction pattern, such that the desired binary phase information is encoded into the hologram. The resulting hologram can be easily implemented using binary optical elements, such as a binary phase-only filter [2].
4. Iterative phase retrieval (IPR): This method starts with an initial guess for the phase information and iteratively refines it until a desired criterion is met. The Gerchberg-Saxton algorithm is a popular IPR method that uses the constraint that the intensity distribution in the object plane must match the desired intensity distribution. The algorithm alternates between computing the intensity in the object plane from the current phase information and updating the phase information based on the measured intensity in the object plane. This process is repeated until convergence is achieved. The final phase information is then used to create the desired hologram [15].
5. Holographic phase conjugation (HPC): This method involves computing the complex conjugate of the hologram and using it as the reference wave in the holographic encoding process. The resulting hologram can be used to form the conjugate of an input wave, which can be used for various applications, such as holographic imaging or beam shaping. HPC is based on the property that the complex conjugate of a hologram reconstructs the conjugate of the object wave. This allows the conjugate of an input wave to be formed by overlapping the input wave with the reference wave from the hologram [16].

2.2.2 Digital holography (DH)

A brief introduction to digital holography is done in this chapter. For detailed information please refer to [17, 18, 19].

Digital holography is a branch of holography that uses digital techniques for the recording, processing, and reconstruction of holograms. Digital holography has several advantages over traditional analog holography, including the ability to process and store holographic information, the ability to manipulate the holographic image, and the ability to display

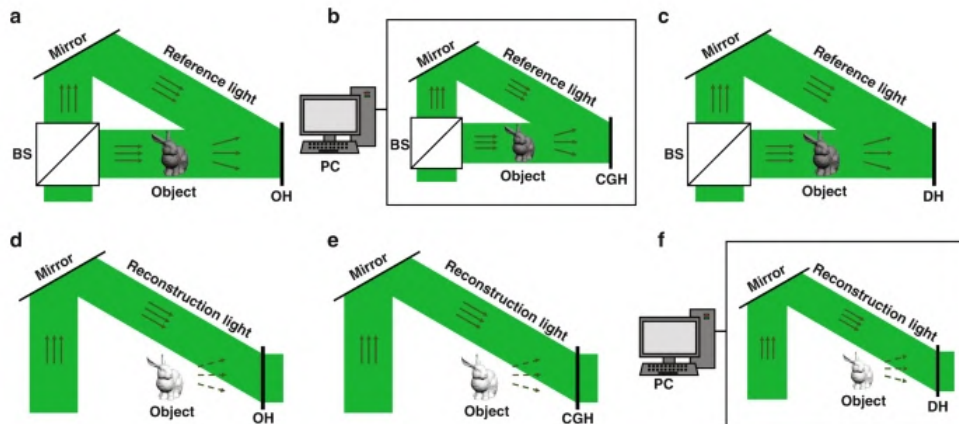


Figure 2.9: a) Obtaining and d) reconstruction of optical holography, c) obtaining and e) reconstruction of computer generated holography (CGH), c) obtaining and f) reconstruction of digital holography (DH) (taken from [14]). The frames with PC mean that part is calculated in the computer.

the hologram on a computer screen. An illustration of analog holography, CGH and DH together is given in Fig. 2.9.

The basic principle of digital holography is similar to that of analog holography, which involves the interference of light waves to produce a hologram. However, instead of using photographic film to record the interference pattern, digital holography uses a digital camera or image sensor to capture the pattern as a digital image [2]. Such sensors can be charge-coupled device (CCD) or a complementary metal-oxide-semiconductor (CMOS) sensor, and the data is processed using digital techniques.

The digital image can then be processed and manipulated using computer algorithms, such as Fourier transform algorithms and image processing techniques, to generate the final holographic image. The reconstructed image can then be displayed on a computer screen or printed on a medium such as a transparency or holographic foil. Below some DH acquisition methods and possible applications are given:

Methods:

1. Digital holographic interferometry (DHI): DHI is a technique used to measure the wavefront of an object, such as a surface or a fluid flow, by interfering the reference wave with the object wave to produce a hologram. The hologram can then be reconstructed and analyzed to determine the wavefront of the object. This allows the *objects* to be analyzed without causing any destruction [20].
2. Digital holographic microscopy (DHM): DHM is a technique used for microscopic imaging, which involves the recording of a hologram of an object using a microscope, and the reconstruction of the hologram to generate a 3D image of the object [21].

DHM can be used for a wide range of applications, including biological imaging, material science, and fluid dynamics.

3. Digital holographic stereo display (DHSD): DHSD is a technique used to produce 3D displays, which involve the reconstruction of a holographic image using two or more holograms recorded from different perspectives [22]. DHSD provides a more immersive viewing experience compared to traditional 2D displays, and has applications in fields such as entertainment, education, and medical imaging.

Applications:

1. Non-destructive testing (NDT): Digital holography can be used for NDT, which involves the examination of objects or materials without causing any damage [24]. DHI can be used to inspect objects such as engineering structures, aircraft components, and pipelines, to detect cracks, defects, or deformations.
2. Medical imaging: DHM can be used in medical imaging to generate 3D images of biological specimens, such as cells, tissues, and organs [25]. DHM provides a non-invasive and high-resolution imaging method, which can be used for diagnostic purposes, such as cancer detection and drug discovery.
3. 3D displays: DHSD can be used to produce 3D displays, which provide a more immersive viewing experience compared to traditional 2D displays [22]. DHSD has applications in fields such as entertainment, education, and medical imaging, as it allows the viewer to experience 3D images in a more natural and interactive manner.

2.3 Spherical harmonics and application of higher order ambisonics

Even though this topic seems out of holography, the relation can be explained as follows. The work to be presented in the further chapters of this study contains an investigation of possible spherical computer generated holography (SCGH) encoding method containing spherical harmonics transform. To be able to understand the presented work, it is important to understand the fundamentals of spherical harmonics and possible applications of it. Higher order ambisonics is one of the areas where spherical harmonics are theoretically and practically applied at a commercial level. Hence, in this section, the theory of spherical harmonics and its application in ambisonics is presented minding that it will later be evolved for holographic applications, as such in chapter 4.

Higher order ambisonics (HOA) is an extension of the basic ambisonics technique that uses more than just the first-order spherical harmonics to encode the sound field. The basic idea behind HOA is to use a higher number of channels to represent the sound field, which allows for a more accurate and detailed representation of the sound field. This

2.3. Spherical harmonics and application of higher order ambisonics

enables highly detailed spatial information reproduction. The sound pressure in free space is represented by the pressure (p) wave equation, [8], which is really similar to the light wave equation:

$$\nabla_{\vec{r}}^2 p(\vec{r}, t) - \frac{1}{c_s^2} \frac{\partial^2 p(\vec{r}, t)}{\partial t^2} = 0 \quad (2.40)$$

where c_s is the speed of sound and $\vec{r} = [r, \theta, \phi]^T$ where θ is the polar angle which ranges from 0 to π , ϕ is the azimuth angle which ranges from 0 to 2π and r is the distance from the center of the sphere.

Basically,

$$p(\vec{r}, t) = R(r)\Theta(\theta)\Phi(\phi)T(t) = p(\vec{r})e^{j\omega t} \quad (2.41)$$

This is true for monochromatic sound sources and from Eq. 2.40, this quickly yields the Helmholtz equation as such:

$$\nabla_{\vec{r}}^2 p(\vec{r}, k) - k_s^2 p(\vec{r}, k) = 0 \quad (2.42)$$

where $k_s = \omega/c_s$ is the wave number of the sound wave. This sound pressure field p can be defined in spherical coordinates by spherical harmonics.

Spherical harmonics are a set of orthogonal functions which can be linearly added to represent a distribution of directional harmonic components of a field in a spherical volume without sources as shown in 2.10.

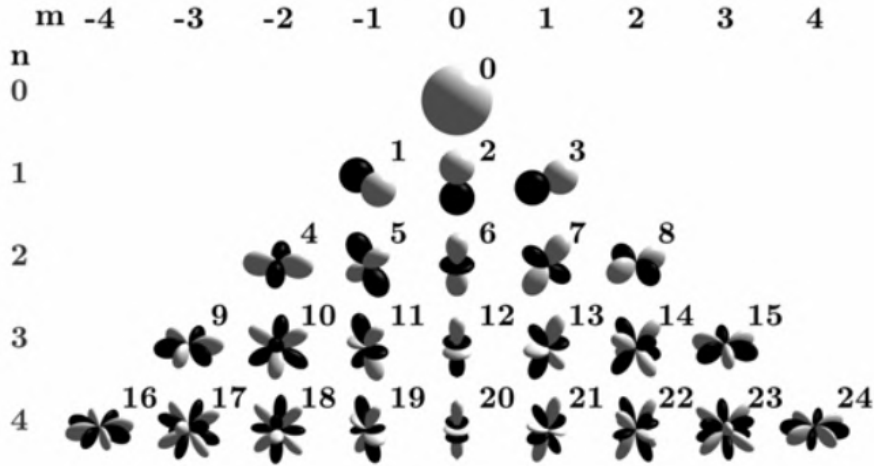


Figure 2.10: Spatial representation of spherical harmonics of order n degree m (taken from [9]).

The sound field is encoded by representing it as a linear combination of spherical harmonics of different orders and for order n there are $(n + 1)^2$ spherical harmonics [8]. The real-valued spherical harmonics is denoted by Y_n^m as,

$$Y_n^m(\theta, \phi) = N_n^m P_n^{|m|}(\sin\phi) \begin{cases} \cos(|m|\theta) & \text{if } m \geq 0 \\ \sin(|m|\theta) & \text{if } m < 0 \end{cases} \quad (2.43)$$

where $P_n^{|m|}$ are the *Legendre polynomials* of order n which supply an orthogonal basis and N_n^m are the normalization function for which there are different implementations, see [8, 9, 10]. The effect of different normalization schemes is researched in [11].

Note: Ambisonics channel numbering (ACN) convention is given in this manner [9]:

$$\begin{aligned} \text{ACN} &= n^2 + n + m \\ n &= \lfloor \sqrt{\text{ACN}} \rfloor \\ m &= \text{ACN} - n^2 - n \end{aligned} \quad (2.44)$$

$$(2.45)$$

which means $Y_n^m = Y_{\text{ACN}}$.

A pressure field p in a sphere volume of radius r_s then can be described with Fourier-Bessel series ([8]) as:

$$p(r, \theta, \phi, f) = \sum_{n=0}^{\infty} i^n j_n(2\pi \frac{f}{c_s r_s}) \sum_{m=-n}^n B_n^m(f) Y_n^m(\theta, \phi) \quad (2.46)$$

where f is the frequency, i is the imaginary unit, and j_n are the spherical Bessel functions of order n . If one knows the spherical harmonics coefficients B_n^m the pressure field can be described. Hence, the pressure field can be *encoded* in a vector of coefficients,

$$b(z) = [b_0(z), b_1(z), \dots, b_{(n+1)^2-1}]^T \quad (2.47)$$

where T is the transpose operator. These coefficients are called Ambisonic coefficients.

There are several ways of decoding Ambisonics coefficients $b(z)$ for regularly and irregularly distributed sound sources [9]. Here regular distribution will be taken into account. The signal for I^{th} sources located at (θ_s, ϕ_s) is given by

$$I(\theta_s, \phi_s, t) = Y_n^m(\theta_s, \phi_s) B_n^m(\theta_i, \phi_i) \quad (2.48)$$

where $Y_n^m(\theta_s, \phi_s)$ are the spherical harmonics for the position of sources and $B_n^m(\theta_i, \phi_i)$ are the encoded Ambisonics coefficients.

State-of-the-Art

In this chapter, related state-of-the-art is analyzed. During the literature review two different areas are deeply investigated, CGH methods and holographic display technologies. The focus for CGH methods is given to cylindrical and spherical CGH methods, and for the display technologies, the light field display has become prominent.

3.1 Methods of computer generated holography

Light field describes the amount of light flowing in every direction through every point in space. To put it more simply, it captures all the light rays traveling in every direction at every point in a scene. Encoding light fields have been under investigation for many years however in the last decades there have been significant improvements. These improvements carry high importance, especially for the computer graphics area in terms of computing, encoding, and manipulating the lighting of a scene. A 2007 study ([26]) successfully analyzed the light source direction and magnitude of a panoramic view by the utilization of spherical harmonics, a results illustration can be seen in Fig. 3.1. The usage of spherical harmonics is parallel to the one explained in Sec. 2.3, the difference is that only the *brightness/illumination* info carries high importance.

In the latest research, it was published that 360-degree holograms were generated with 45 degrees of off-axis viewing angle using spatially multiplexing 2×2 dot matrix display arrays and utilizing mechanically rotating optical components [22]. An illustration of the system is given in Fig. 3.2. This system is able to generate 20 frames per second 3.2-inch dynamic holograms. A similar approach with heavy utilization of FFT and multiplexing in the spatial domain has been followed for 360-degree tabletop holograms by the same authors in [23].

Although this system constitutes a solid improvement, mechanical rotation is not a safe choice to go with as the calibration might be hard to achieve. Another problematic part is that although it is 360 degrees the viewing angle is still limited. However, since the system is considered to be on a tabletop, having the view zone only at the top of the hologram is not considered to be a problem.

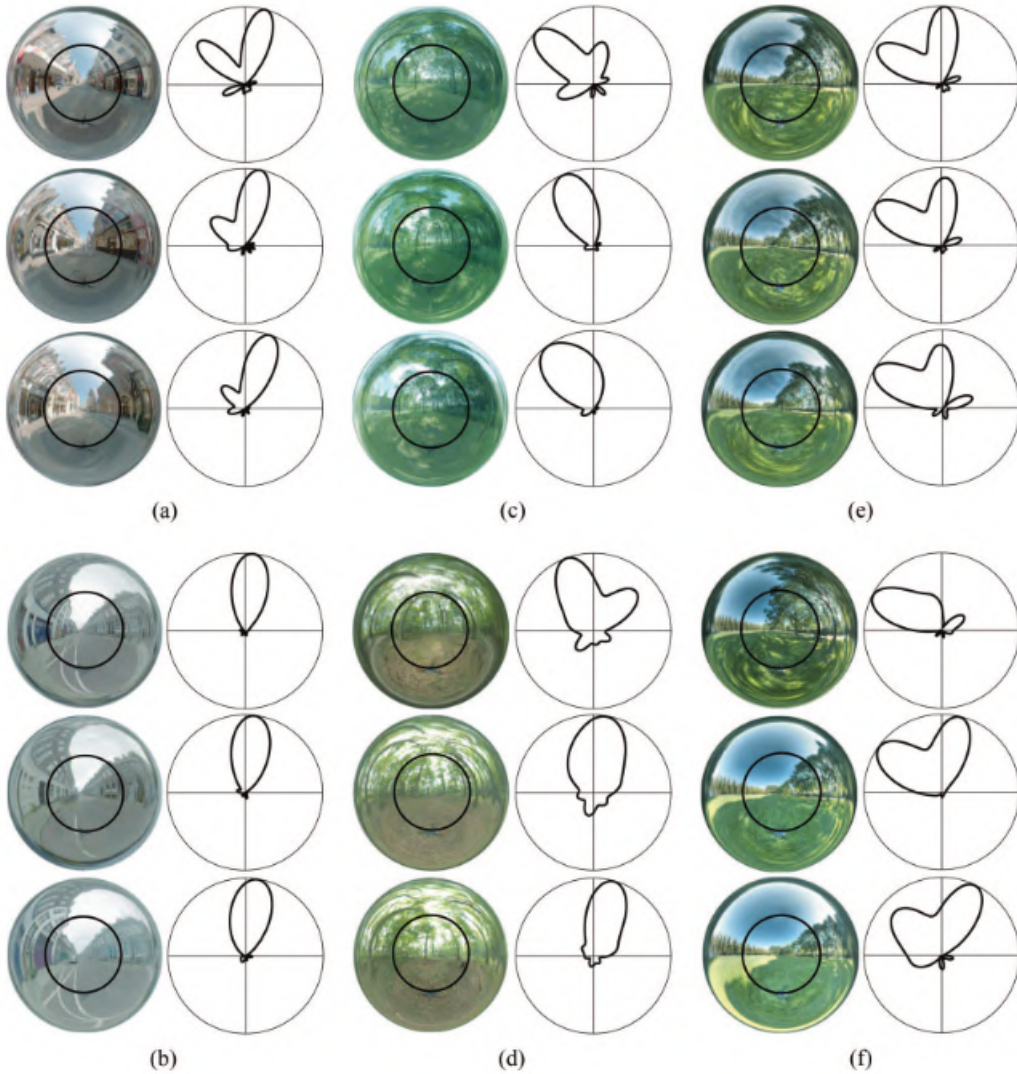


Figure 3.1: Light fields of different scenery are encoded with spherical harmonics. The directional curves indicate the direction that the panoramic images are enlightened from (taken from [26]).

In a 2020 research [27], a fast diffraction calculation method between a plane and a sphere for spherical computer-generated holography (SCGH) based on phase compensation (PC) is proposed. This method consists of two steps: first, recording the optical field from the object plane in a wavefront recording plane (WRP), using the conventional plane-to-plane diffraction calculation method; second, compensating the phase difference between WRP and SCGH by approximating it point-to-point to generate the SCGH. The PC method offers several advantages over the original point source (PS) method, including fewer sampling points, good scalability, and faster computing speed. The proposed

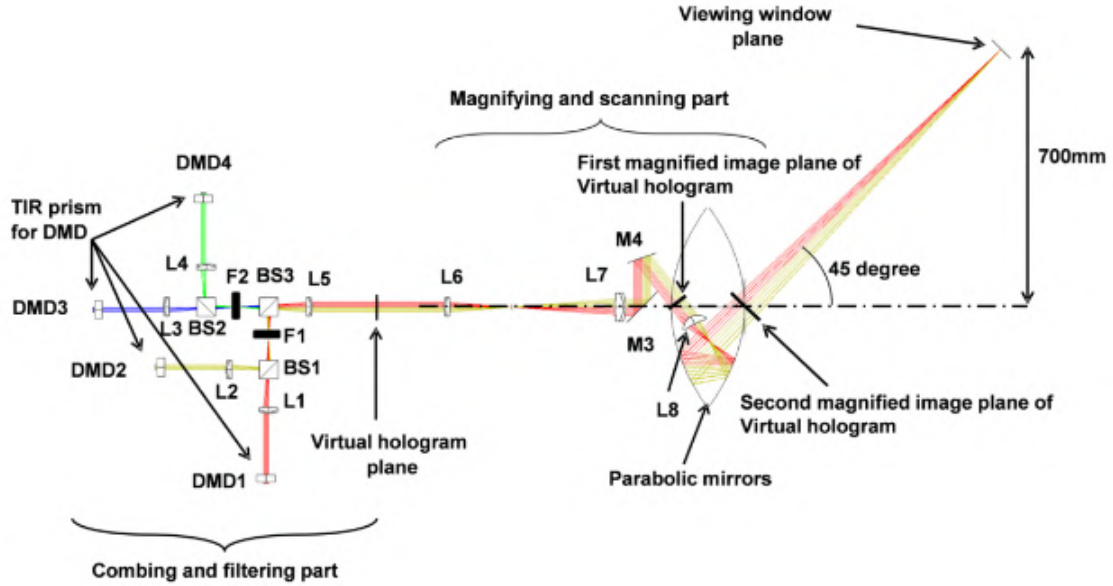


Figure 3.2: System illustration built within the research presented in [22]. L: lens; BS: beamsplitter; F: optical filter; M: mirror; C: collimator. The colors are for ray tracing (taken from [22]).

method was verified through numerical simulations and optical experiments, and its feasibility, error, and performance were analyzed. Despite being an approximate method, the quality of the reconstructed images was still good even with increased curvature of SCGHs or resolution of the object planes. Additionally, a new approach using the PC method to perform optical experiments of SCGH was provided by compensating the phase difference between the SCGH and the planar spatial light modulator (SLM) before loading the hologram onto the SLM for reconstruction, making it closer to practical applications of spherical holography. A graphical illustration of the system is given in Fig. 3.3.

In 2017 research [28], a fast calculation method for spherical CGH using spherical harmonic transform is presented. The method involves transforming a 3D object in the Cartesian coordinate system using fast Fourier transforms (FFTs) and extracting Fourier components on the spherical surface of radius $1/\lambda$. The wavefront on the spherical surface is calculated from the spherical Fourier components and the diffraction integral between the components and the wavefront is expressed as a convolution integral on the sphere, which can be calculated quickly using spherical harmonic transform through an open-source library (SHTOOLS). The validity and effectiveness of the method have been verified through numerical simulation, see Fig. 3.4. The method overcomes the limitations of conventional planar CGHs (very limited viewing angle) and cylindrical CGHs (360 on the sides, however same limitation as planar CGHs in the vertical direction) in terms of viewing zone and calculation time. The total time to calculate the diffracted wavefront from the 3D

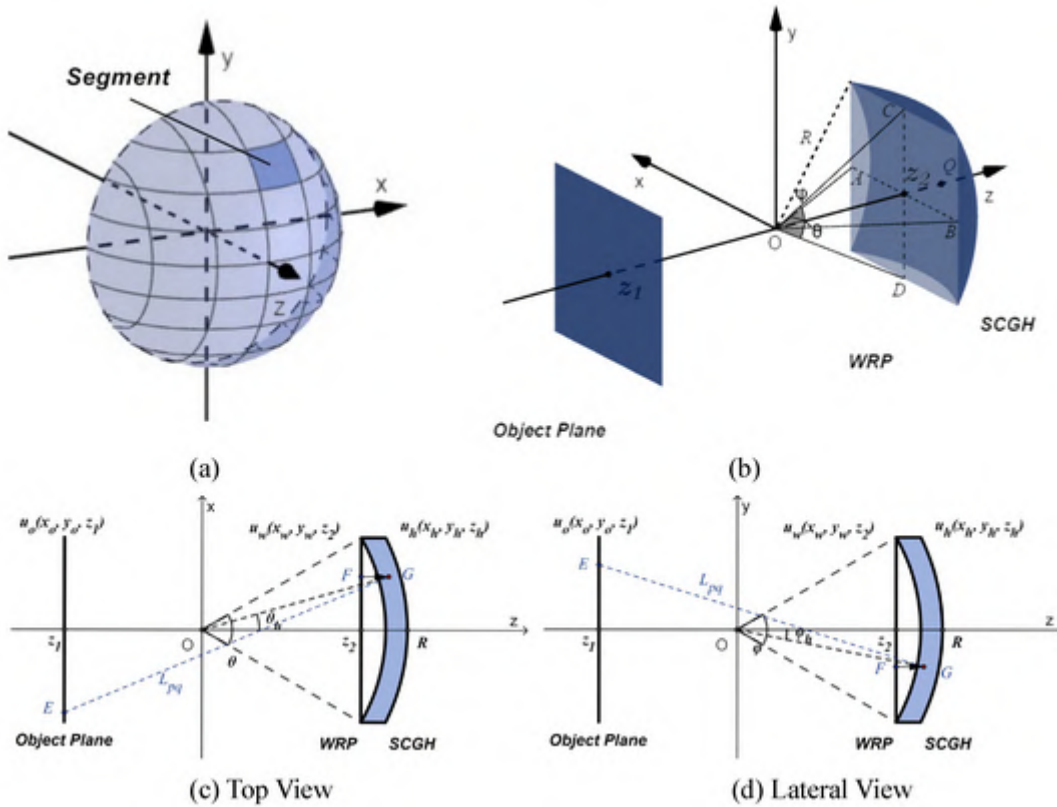


Figure 3.3: Figures (a and b) depict the propagation model between a plane and a sphere, while figures (c and d) show the schematic of SCGH generation using the phase compensation (PC) method (taken from [27]).

object was approximately 5.4 seconds whereas it was approximately 4,900 seconds in the direct calculation method which calculated directly the superimposition of the spherical waves emitted from all the object points [28]. A question can be proposed here as the used wavelength for the simulation is $44 \mu\text{m}$ which is considerably far away from the visible spectrum ($0.4 - 0.7 \mu\text{m}$). It has been stated that for simulation purposes, this is fine however no further explanation is given.

The cylindrical holograms and SCGH are being heavily researched. However, one of the biggest setbacks is the computation time for the algorithms. In recent research, calculation time and resolution improvements are proposed in [29, 30]. Occlusion culling is disregarding the parts that are overlapping from the perspective of the observer and can not be seen. If not disregarded this causes higher computation times and eventually ends up cluttering the final image, especially for complex 3D objects. The main idea in papers [29, 30], is that they came up with a solution to stop these parts from being computed which reduces computation time and the noise in the reconstructed image. In [29] the method proposed considers both the object-image-plane (OIP) and image-object-plane (IOP) models of light propagation and limits the diffraction area of each source point within the corresponding

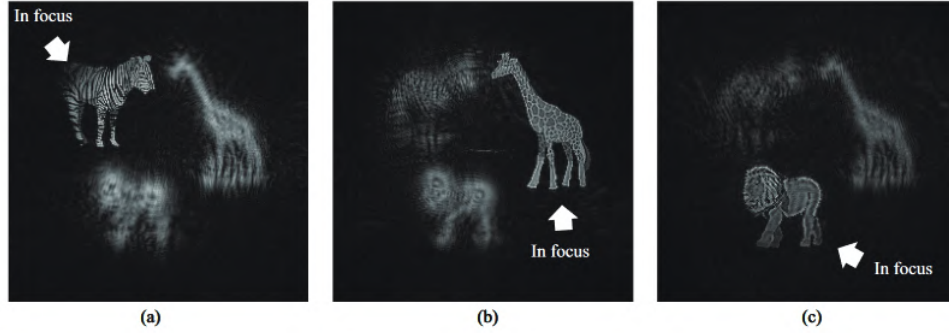


Figure 3.4: Reconstructed images are given. (a), (b), and (c) represent the reconstructed images there are at different depths, respectively at $z = -2.5$ mm, 0 mm, and 2.5 mm (taken from [28]).

tangents. The authors use a line light source to illuminate the selected source points and observe that the diffraction area is independent of the z -axis coordinate. The authors then propose the use of a horizontal optical path filter (HOLF) embedded in the point spread function (PSF) to achieve occlusion culling. The HOLF determines whether the light ray should be retained or removed by multiplying the PSF by 1 or 0, respectively. The new PSF is then calculated by multiplying the PSF by the HOLF. The authors establish the HOLF based on the difference in angular coordinates between the source and destination points, and the size of the cylindrical object. The horizontal optical path is calculated, and if it is less than or equal to the square root of the difference between the square of the inner and outer cylinder radii, the HOLF is set to 1. Otherwise, it is set to 0. In Fig. 3.5 and Fig. 3.6, illustrations are given on calculation, and the actions taken for these situations are given.

On the other hand, in [30] the occlusion method is not detailed but mentioned that the image is rendered for a certain direction and the occluded parts are just discarded. However, the usage of SHT and the occlusion culling has been analyzed in terms of calculation time which has been demonstrated to be improved drastically compared to direct point-by-point calculation, the results are shown in Fig. 3.7.

There has been a rapid rise in the development and application of CGH based on Deep Neural Networks (DNNs). Various deep learning-based CGH methods have been proposed and implemented. For example, [31] proposed a deep ResNet for calculating holograms in 2018, and [32] proposed a U-Net-based architecture for generating binary holograms in 2020. In 2020, [33] presented a multi-depth hologram generation network (MDHGN) for reconstructing 3D images. [35] proposed a new algorithm called DeepCGH, which was a U-Net with five convolutional blocks, for hologram synthesis. In 2021, [34] proposed a non-iterative 3D CGH method based on ResNet and U-Net, and [36] proposed the concept of tensor holography for true 3D color holography.

The results of these studies have shown that deep learning networks can improve the

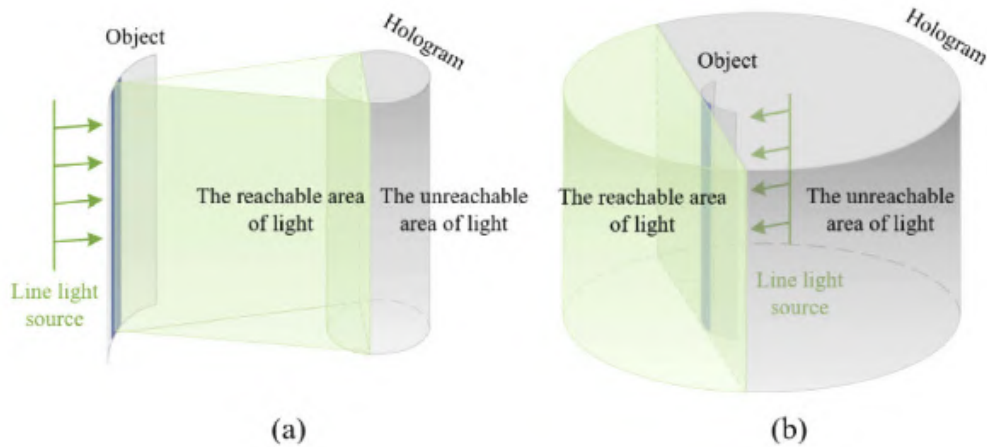


Figure 3.5: Schematic diagram for (a) object-image-plane and (b) image-object-plane methods (taken from [29]).

accuracy and processing speed of holographic image reconstruction compared to existing methods like Gerchberg-Saxton (GS) and NOVO-CGH algorithms. These deep learning-based CGH methods have been implemented using programming languages like Python and frameworks like TensorFlow, widely available and studied.

3.2 Display technology and volumetric displays

In this section, the latest display technologies for holography are briefly investigated. Properly displaying holograms has been a strong focus of holographic research. Projecting high-quality three-dimensional (3D) scenes via computer-generated holography would create many benefits for virtual and augmented reality, human-computer interaction, and many more areas.

Common solutions to display technology include stereoscopic displays with tracking. Stereoscopic displays [41] can only emit two unique light beams per pixel, leading to limitations such as the need for the viewer to be in a specific position (the sweet spot), viewer-dependent views, or tracking requirements [42] to create motion parallax, which currently only supports single or a few users and is prone to inaccuracies and latency.

Multi-view systems can create 8-16 views [43], but this is still significantly limited, resulting in a jumpy visual experience, a restricted field of view, and invalid zones. These systems usually use 2D panels as their foundation, which presents a trade-off between direction and resolution: introducing n directions reduces the resolution by a factor of $1/n$. This is particularly evident with integral imaging, where the vertical views also consume available resolution, effectively making integral imaging a full-version multi-view

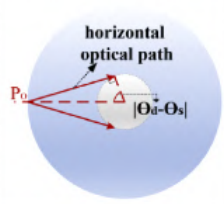
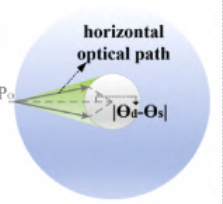
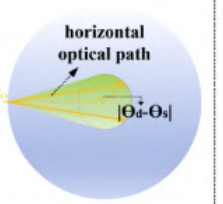
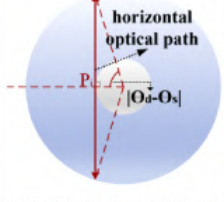
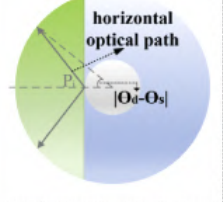
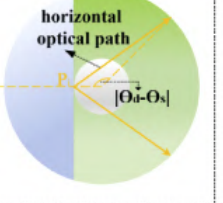
d_{op}	$d_{op} = \sqrt{(R^2 - r^2)}$	$d_{op} < \sqrt{(R^2 - r^2)}$	$d_{op} > \sqrt{(R^2 - r^2)}$
OIP			
IOP			
Method	retain	retain	remove

Figure 3.6: Correspondence between light and processing methods (taken from [29]).

system with vertical parallax.

Volumetric systems diverge from the usual display conventions, adopting a 'looking into' rather than a 'looking out' philosophy [56]. Just like other systems, the global number applies to volumetric systems, representing the number of addressable spatial spots. However, this approach results in an occlusion issue. Since light doesn't cover light, bright spots in the background are always visible, and there's no method to display natural scenes with hidden edges—only translucent images or wireframes can be shown [56].

Holographic systems, on the other hand, create holographic patterns to reproduce the wavefront [56]. These systems have inherent limitations on feasible image sizes, viewing angles, and they don't have unlimited resolution in the field of view. When using the same image as the base, the total number of spots that can be produced by diffractive or refractive imaging remains the same. However, in practice, holographic solutions demonstrate inferior performance due to the limited phase modulation abilities of current components [56].

The solutions focused on here are not holographic displays that are utilizing interference but rather ones that use light field, still taking an approach of holographic geometrical principles. Some commercial announcements are briefly explained below.

3.2.1 SeeReal Technologies and holographic displays

The company¹ aimed to reconstruct only that part of the wavefront originating from the object that reaches the eye pupils of an observer. This approach is a vertical-parallax-only

¹<https://seereal.com/>

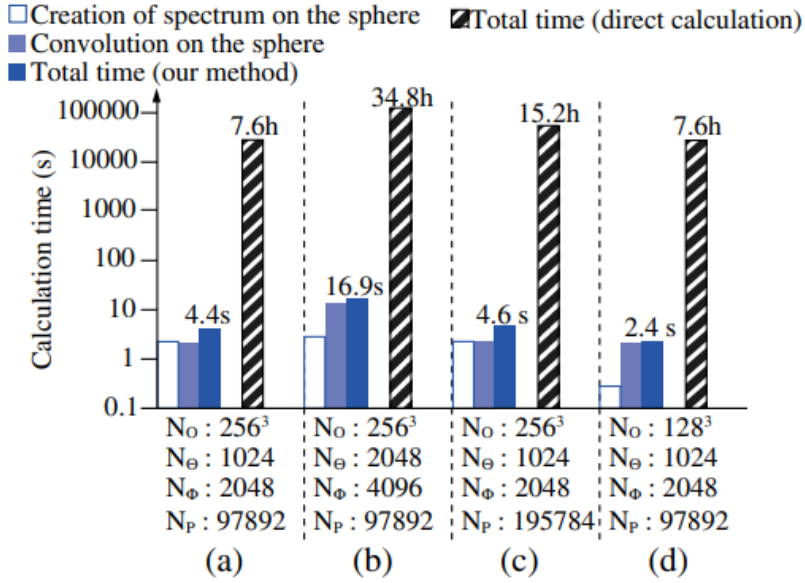


Figure 3.7: Calculation times required under the various conditions, N_O , N_Θ , N_Φ , and N_P represent sampling numbers of the object space, Θ , Φ , and the number of point light sources constituting the 3D object, respectively (taken from [30]).

system, where a wavefront in a small region, termed the "observer window," is reconstructed.

The observer window's size is related to the size of the eye pupil and may be located in the Fourier plane of the hologram. For each eye, a separate observer window is created either by spatial or temporal multiplexing, hence, the observer window's size determines the pixel period needed on the display. This concept is closely related to the sub-hologram, a limited hologram region associated with the positions of an object point and the eye pupil.

A monochrome real-time prototype was built using a 20-inch monitor in 2007. The prototype achieved a holographic reconstruction of the wave field at the observer's eye position using a relatively large pixel size. The viewing window and diffraction angle are quite small due to the large pixel size of the SLM, but a large reconstruction can be displayed over a wide depth range of about 4 meters [44, 45, 46, 47].

3.2.2 QinetiQ and the Active Tiling system

QinetiQ¹ developed the Active Tiling system [48], designed to leverage the high frame rate of electrically addressed SLMs (EASLMs) and the non-pixelated structure of optically addressed SLMs (OASLMs) [49]. This innovative design enables significantly higher pixel counts while maintaining overall video update rates.

¹<https://www.qinetiq.com/en/>

The system includes an EASLM that acts as an "image engine," capable of rapidly displaying computer-generated hologram (CGH) image elements. A replication optics set projects multiple de-magnified images of the EASLM onto an OASLM. The OASLM stores and displays the computer-generated pattern. A control system synchronizes the entire system.

A typical Active Tiling configuration uses a ferroelectric crystal on silicon (FLCoS) EASLM with 1024×1024 binary pixels and operates at a 2.5-kHz frame rate. The system can display images with a pixel count in the order of 10^8 [50].

3.2.3 HoloVizio

The HoloVizio technology from Holografika¹, which is patented, utilizes a carefully organized array of optical modules and a holographic screen [56]. Each point on the holographic screen projects light beams in varying colors and intensities in multiple directions. These light beams, created in the optical modules, strike the screen at different angles, and the holographic screen performs the required optical transformation to integrate these beams into a seamless 3D view [56]. With appropriate software management, light beams departing the pixels move in numerous directions, mimicking the emission from 3D objects at specific spatial positions. The need for direction-selective light emission is universal across all 3D systems and provides numerical information about the field of view, the angular resolution, which in turn determines the field depth of the displays, and affects the total quantity of necessary light beams for advanced 3D display [56].

This system is an effective demonstration of the Light field displays (LFDs) and a more detailed explanation of LFDs is given in the next section (sec. 3.3).

3.3 Light field display technology

The landscape of visual technology is constantly changing as researchers and companies push the boundaries of what is possible in the pursuit of more immersive, realistic experiences. LFDs, a sophisticated class of display systems that can provide an extraordinarily natural viewing experience by recreating the full range of light entering the eye from a 3D scene, are one such development [52]. This technology has the potential to revolutionize fields such as virtual and augmented reality, scientific visualization, and remote collaboration, to name a few.

3.3.1 Plenoptic function

All of the visible world consists of light and rays that are reaching to our eye. When we place a pinhole camera at a spatial location defined by coordinates (x, y, z) , it captures a distinct set of rays passing through that location and they can be noted as $P(x, y, z)$ [68]. The directionality of rays' intensity can be illustrated using spherical coordinates, denoted

¹<https://holografika.com/>

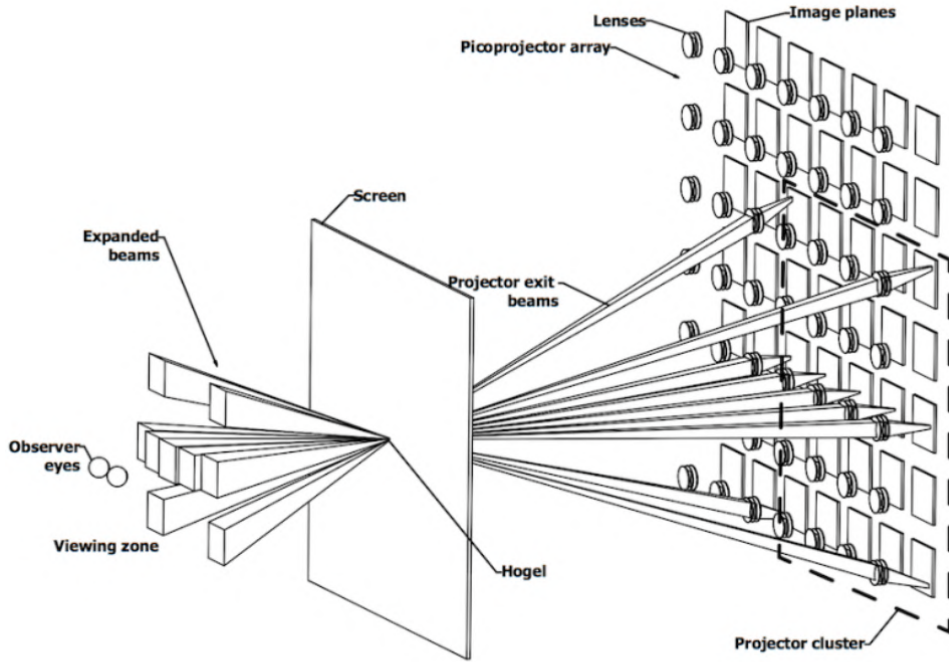


Figure 3.8: LFD layer by layer decomposition illustrating the working principle (taken from [59]).

as (θ, ϕ) , broadening the set definition to $P(x, y, z, \theta, \phi)$. By including color, and therefore considering intensity variations across different wavelengths λ , we expand this definition to $P(x, y, z, \theta, \phi, \lambda)$. When capturing a scene that changes over time, a time dimension is incorporated, leading to the function $P(x, y, z, \theta, \phi, \lambda, t)$, which is widely recognized as the plenoptic function [68].

While holograms deal with all aspects of light including polarization and phase to the plenoptic function, LFDs are dealing only with five points of the plenoptic function $P(x, y, z, \theta, \phi)$ which is known as light field.

3.3.2 Technical explanation

The light field theory, which describes light intensity distribution in three dimensions, is the underlying principle behind Light field displays. The amount of light traveling in each direction through each point determines the intensity of light at each point in space, according to this theory. Because traditional 2D displays can only display light in two dimensions, they are incapable of reproducing the depth of a scene, severely limiting their ability to recreate realistic three-dimensional scenes [54].

Light Field Displays work by using an array of micro-lenses and/or other optical ele-

ments to project light in a variety of directions, effectively creating a volumetric image. This array is placed in front of the display panel, which generates the projected light. Each micro-lens collects light from a small area of the display panel and directs it in multiple directions, resulting in the creation of a miniature image [56]. An illustration of such a system can be seen in Fig. 3.8.

The human eye perceives these multiple mini-images as a continuous image, allowing the viewer to perceive depth without the use of any additional devices. This depth perception is achieved because the eye receives a slightly different image depending on the viewing angle, just as we do in the real world. This allows them to create realistic three-dimensional images that can be viewed from any angle resulting in a more natural, immersive viewing experience [55].

There are numerous approaches to implementing a Light field display, each with its own set of advantages and disadvantages. Lenslet-based displays, holographic displays, and multi-layer displays are the most commonly used technologies. Each of these employs a unique mechanism to produce the effect of displaying different images depending on the viewing angle [56].

3.3.3 Possible usage of LFDs

Light Field Displays have a wide range of potential applications. They can be used to provide a more immersive and realistic experience in virtual reality systems, allowing users to interact with virtual objects as if they were real. Similarly, they can be used to provide a seamless blend of virtual and real objects in augmented reality systems.

Furthermore, Light field displays have potential applications in medical imaging, where they could allow doctors to visualize complex 3D structures like organs and tissues in a much more natural and intuitive manner. They could also be used in remote collaboration tools to allow users to interact with 3D models or environments in a shared virtual space [57].

3.3.4 Looking Glass Portrait

Looking Glass Factory¹, a market leader in LFD technology has recently released Looking Glass Portrait, a consumer-grade light field display device. This commercial holographic display is intended to provide users with a window into the digital world, allowing for levels of immersion and interactivity not previously possible with traditional display technologies [58].

Looking Glass Portrait² (LGP) makes use of lenticular lens display technology, which employs a series of micro-lenses to project different images depending on the viewing angle. An example of a lenticular lens array can be seen in Fig. 3.9. As a result, a 3D image can be viewed from various angles without the use of additional devices such as glasses or

¹<https://lookingglassfactory.com/>

²<https://lookingglassfactory.com/looking-glass-portrait>

headsets. Furthermore, the device employs a high-resolution display panel to ensure sharp and clear 3D images [58]. It is able to create up to 100 seamlessly transitioning views in a 58-degree horizontal viewing cone with a 4:3:2 (H:L:D) aspect ratio and a resolution of 1536×2048 [58]. The device can be seen in Fig. 4.13.

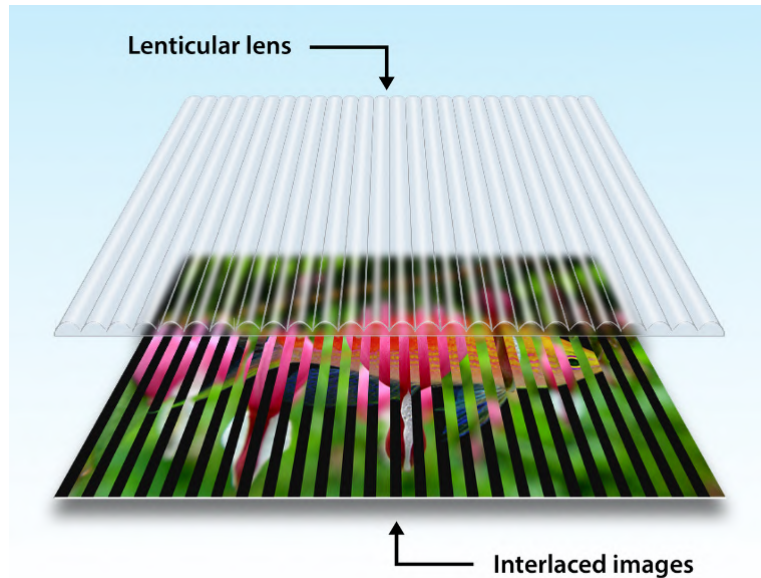


Figure 3.9: Generic lenticular lens array (taken from [60]).

LGP can show both static and animated 3D content. It can be used to display 3D models, animations, or even 3D photographs, giving users a novel and engaging way to interact with digital content. It also includes a set of software tools that allow users to create, edit, and display their own 3D content, opening up a world of creative possibilities [58].

3.4 JPEG Pleno database

Certain tools and libraries are needed for this task such as a holographic image database, software to reconstruct the images, software to control the process, and LGP. JPEG Pleno database¹ and numerical reconstruction software for holography become really handy for this as they are parallelly maintained. So in this section first the JPEG Pleno Database, the reconstruction software will be explained in detail, technical aspects of the used LGP will be briefly described, and finally, the proposed workflow and the software will be demonstrated.

The JPEG Pleno² framework is an initiative of the JPEG committee to standardize the representation and exchange of plenoptic content. The JPEG Pleno database was created

¹<http://plenodb.jpeg.org/>

²<https://jpeg.org/jpegpleno/>

to provide test data for the development of this new standard, and it includes a variety of plenoptic content modalities such as light fields, point clouds, digital holography, and more [63].

The JPEG Pleno database is a valuable resource that includes several modalities, each with its own set of specifications. These datasets are primarily used to test and validate the JPEG Pleno standardization framework's efficiency. This standard is intended to make it easier to compress these datasets, which are typically large and complex due to the rich information they contain [64].

The datasets in the JPEG Pleno database cover a wide range of applications. In general, each dataset is structured to include specific technical parameters that define its use and functionality. Depending on the modality, this can include resolution, depth of field, dimensions, viewing angles, and more [64].

3.4.1 Datasets for holography

The digital holography dataset, which is essential for the development of holographic applications, is one modality in the JPEG Pleno database. Several specific parameters characterize holography datasets, such as the wavelength of the light used, the angles of the reference and object beams, and the distances from the object and the reference point to the hologram. Furthermore, the phase and amplitude of the light wave at each point in the hologram are described in these datasets [65].

Furthermore, each holography dataset contains complex-valued hologram samples, each of which represents a holographic fringe corresponding to a point in the 3D object scene. This effectively spatially and spectrally multiplexes holographic data, capturing the full field (amplitude and phase) of the light wavefront scattered from the object [65]. These files are represented as either amplitude and phase information or imaginary and real parts of the hologram in high-definition image files (exr format), an example of data can be seen in Fig. 3.10¹.

3.5 JPEG Pleno numerical reconstruction software for holograms

Digital reconstructions of numerical holograms allow for data visualization and can be used for everything from microscopy to holographic displays. The numerical reconstruction software for holograms (NRSH) ² is an open-source MATLAB³ toolbox that reflects the best current agreement that was produced as part of the JPEG Pleno holography standardization initiative [61]. It is capable of processing Fresnel, angular spectrum, and Fourier-Fresnel holograms with one or more color channels, as well as diffraction-limited

¹For possible printing issues: The image contains red, green, and blue speckles and there are 2 blurry silhouettes visible representing the ballets

²<https://gitlab.com/wg1/jpeg-pleno-nrsh>

³<https://www.mathworks.com/products/matlab.html>

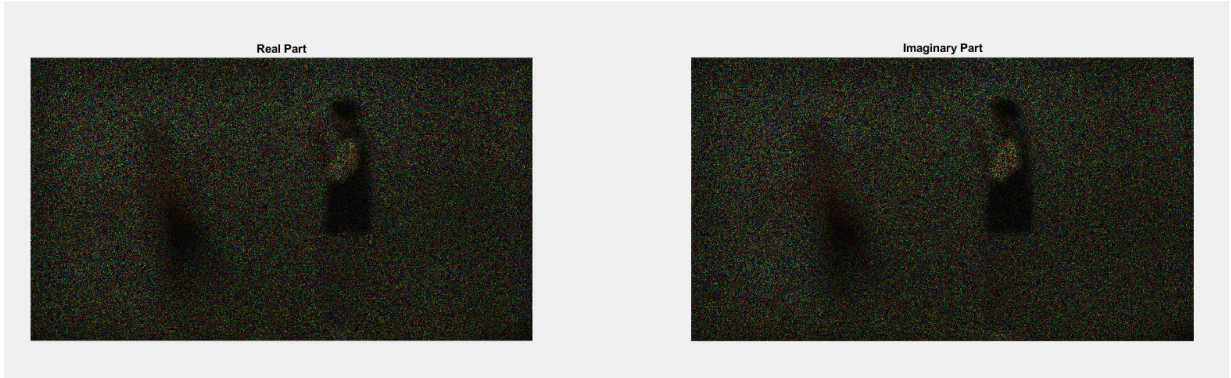


Figure 3.10: Holographic image data that is contained in ballet8k4k frame 22 holographic image in BCOM dataset. On the left real part of the hologram and on the right the imaginary part of the hologram is represented.

numerical reconstructions. The latter allows for the reconstruction of holograms at their intrinsic physical resolution rather than an arbitrarily determined numerical level [61]. The workflow of the published software can be seen in Fig. 3.11. All big public data sets presented by UBI, BCOM¹, and ETRI² are supported in their native and vertical off-axis binary versions [61]. The property of supporting publicly available holography datasets, creates a unification of hologram processing eventually easing up the creation of unified applications for hologram conversion and display technologies.

3.6 Light field and holography correlation and conversion

This section discusses the conversion techniques between Light Field and Holography, two complementary modelling methods of scene lighting [66]. The former represents the scene using rays while the latter uses waves [67]. While most methods are geared towards conversion from light field to holography, the conversion can theoretically be implemented both ways [68]. The main challenge in such conversion is the differentiation between coherent and incoherent light. Holograms capture coherent light, while light fields generally use incoherent light [69].

One of the widely-used conversion methods involves the computation of an object wave for the generation of a Computer generated holography (CGH) [70]. This point-source approach views isolated points as spherical light sources to describe a 3D scene analytically. The summation of the waves scattered by each point yields the desired object wave. Another approach, the wave-field method, uses depth layers parallel to the hologram plane to emit a complex wave [70].

¹<https://hologram-repository.labs.b-com.com//holographic-images>

²<https://etri.gov-dooray.com/share/drive-files/kdhawuidbrbd.1-LdD-NFS1SCrVoykkFg9g>

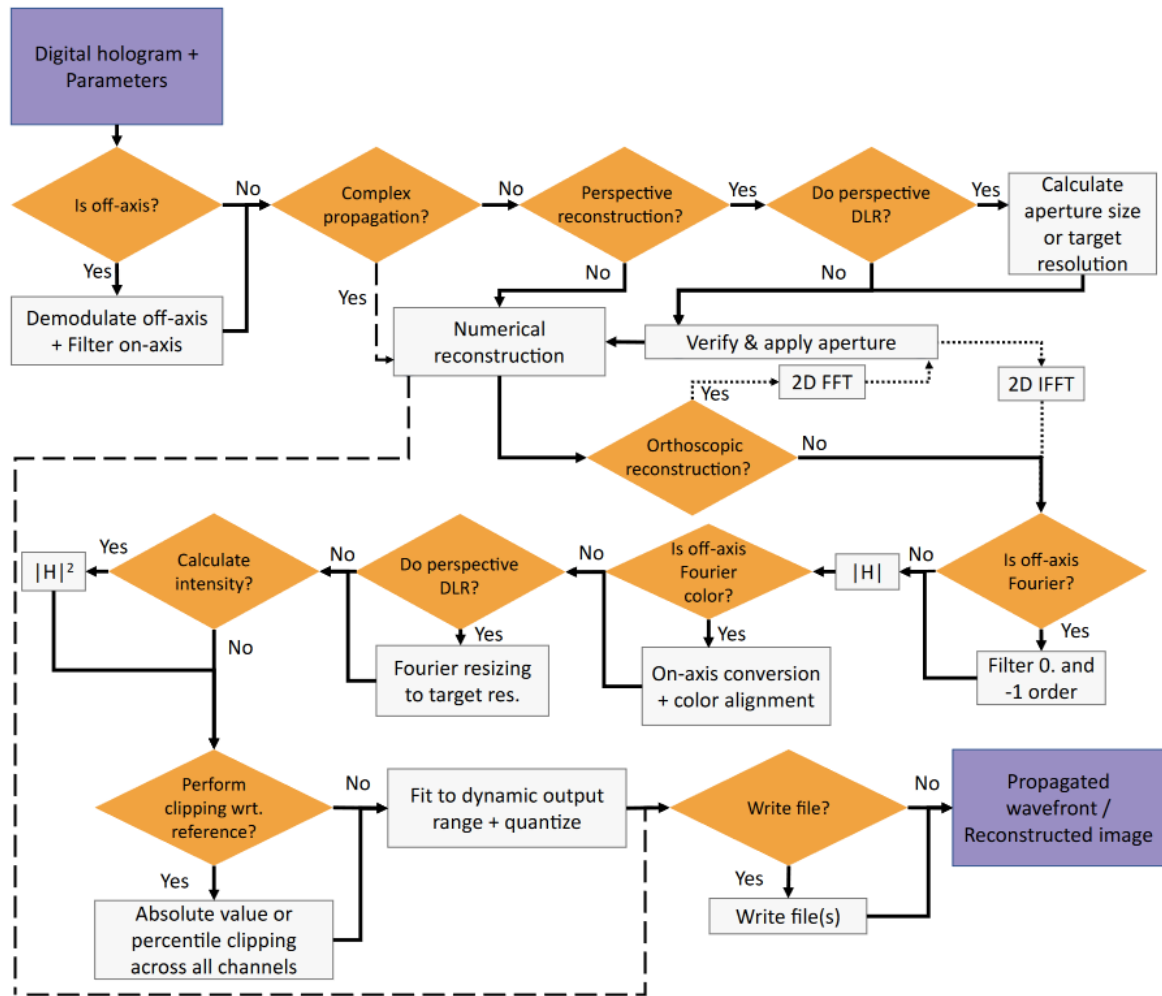


Figure 3.11: JPEG Pleno numerical reconstruction software for holography workflow (taken from [61]).

For cases with a large scene depth, the computational time would need to be considerable due to the required number of depth layers. To address this, a technique based on polygonal modeling has been proposed that utilizes a set of oriented polygons as surface light sources [71].

An alternate method, Multiple-viewpoint projection, computes the object wave from a set of multi-view images [70]. This method generates "coherent" holograms when the 2D view projections of the scene are supplemented with depth maps or synthetic 3D [34]. For real, incoherent cases without additional depth information, the object wave is computed by multiplying each view by a given point spread function (PSF) and summing them together [70].

3. STATE-OF-THE-ART

In the Phase reconstruction approach, the phase of the final hologram is retrieved from a set of defocused images. While in both the holographic stereogram approach and the Wigner distribution function approach, hogels are used with the final hologram being a combination of these [72, 73].

A Method to Encode and Display Holograms

In this chapter, a method to encode and display holograms is discussed. This method consists of a pipeline that starts from 3D object data in cartesian coordinates and ends at the displaying of the holograms. For the displaying of the holograms, there are two different conceptual approaches are presented and one of them is realized. The organization is given in a way that first an overview of the pipeline is presented and then the parts of the pipeline are explained in their relative sections.

4.1 Introduction to the method

CGH is a hard area that consists of many parts such as encoding, processing, and displaying holograms, all of which are challenging tasks. These tasks are gathered and implemented in different combinations and over the years many methods have been proposed and some of the methods have been explained in the chapter 3. The encoding method that achieves the widest field of view (FOV) without any moving parts has been cylindrical CGH, which lacks vision in the vertical angles [29]. Spherical CGH supplies the possibility of having an unlimited FOV around the sphere in theory, yet it stays far away from practical applications for now. On the other side, FOV-limited holographic displays are practically and commercially available, even can be on the top of your desk [58]. Moreover, the advancement of publicly available reconstruction algorithms and datasets for holography [61, 64], enabled the construction of holographic frameworks and ease up the development of holographic processing methods [65, 66, 67].

The method proposed here tries to gather these aspects and present a comprehensive solution for CGH in light of state-of-the-art theoretical and practical approaches. In the construction of this method, three key concepts are utilized, SHT for encoding and processing [30], NRSR for reconstruction [61], and LFDs (specifically LGP) for displaying. Detailed explanations are given in the related sections under this chapter.

4. A METHOD TO ENCODE AND DISPLAY HOLOGRAMS

The method has been divided into two main parts, encoding the hologram and displaying the hologram. The processing of the hologram in terms of manipulations to the encoded material is included in the encoding part. The pipeline is shown in Fig. 4.1.

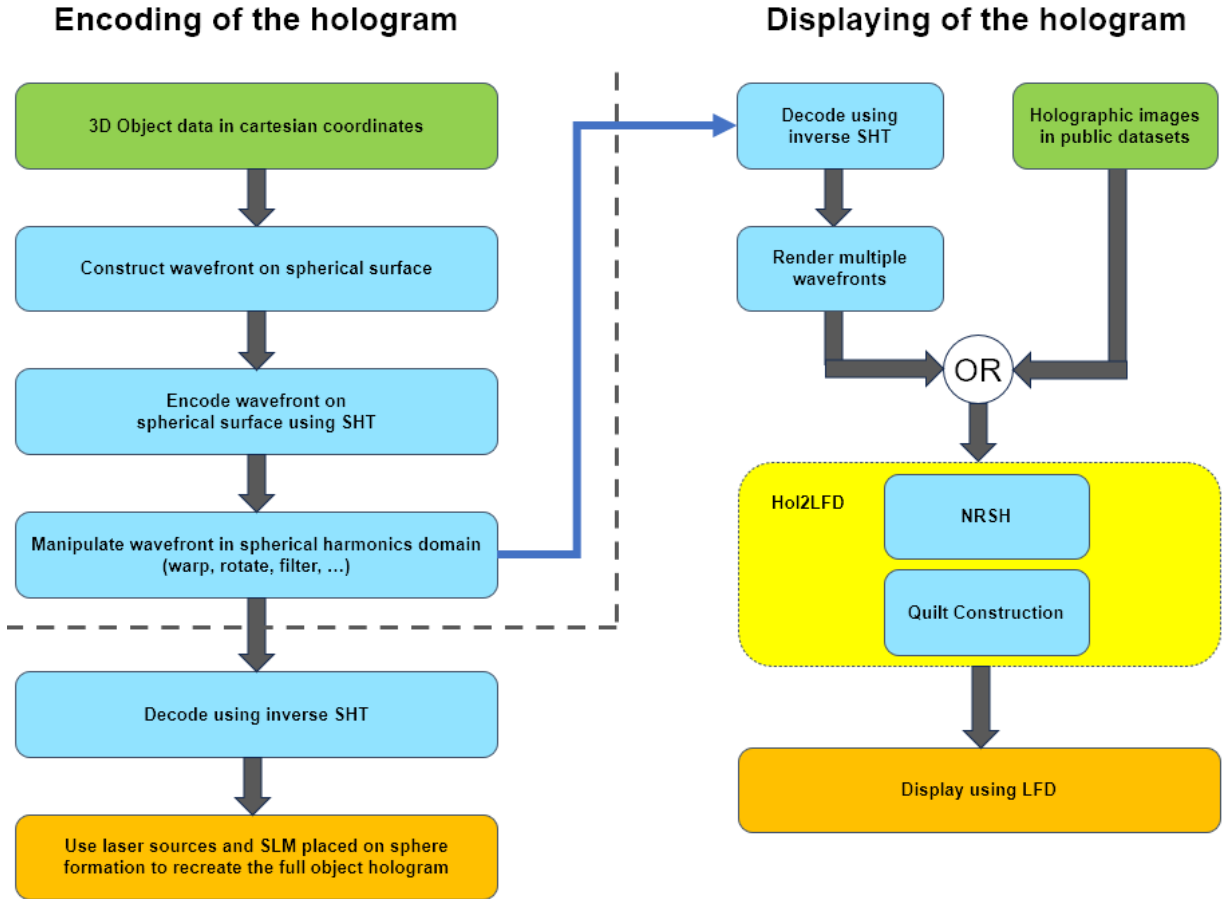


Figure 4.1: Block diagram of the proposed method. The method is divided into two parts. On the left of the dashed line, the encoding of the objects is shown and on the right of the dashed line, the displaying of the holograms is shown. The external inputs to the system are given in green color, the intermediate steps are given in turquoise color, and the outputs of the system are given in orange color. The yellow-colored box indicates the implemented system Hol2LFD.

Detailed reasoning of the workflow In the proposed method, the encoding of the hologram starts with a 3D object located in space which is representable in the cartesian coordinates. This object diffracts a wavefront on a spherical surface around it, this diffracted wavefront can be calculated. Spherical harmonics enable a very efficient description and encoding of the diffracted wavefront by converting huge amounts of data values on the spherical surface to very few spherical harmonics coefficients. These coefficients rep-

resent the amplitudes of orthogonal Legendre polynomials which can be multiplied with these coefficients and added together to describe complex functions on the spherical surface. These coefficients are calculable through SHT. The special transform matrices in the spherical harmonics domain are already prepared for the manipulation of these sound signals [7, 8, 9, 10], and these matrices contain rotation and filtering of the sound field. The same procedure can be applied to encoded wavefronts because the transform matrices essentially compute the rotation of the combination of Legendre polynomials. Since SHT is a reversible transform, the inverse SHT is easily calculable, hence decoding the processed/manipulated wavefront. Decoding and displaying are approached in two ways here.

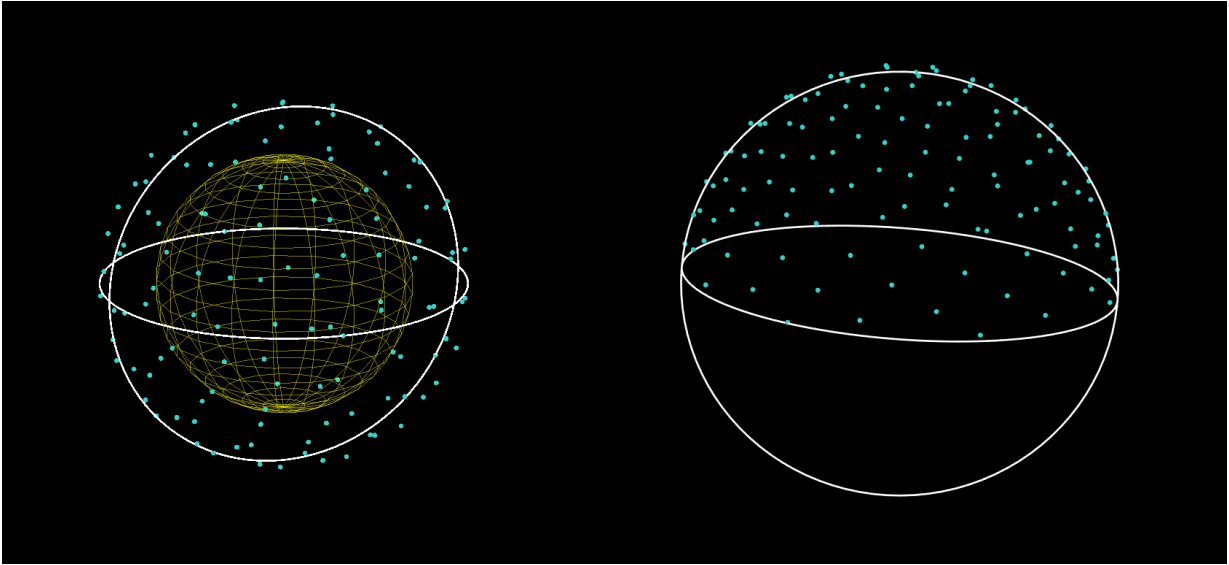


Figure 4.2: Equidistant laser distribution on a spherical and hemispherical surface, the tiling structure is also illustrated on the spherical surface.

The first approach is full spherical decoding. In Ambisonics, the decoded signal contains $(N + 1)^2$ channels based on the SHT order N . Although in Ambisonics this represents speaker feeds [7], it is ambiguous in our case. However, taking stem from the similarities between light and sound waves (see section 4.2.1), This might also represent the laser points feeds, however further processing stays certain to be necessary. Still, a preliminary design can be suggested as equally spaced $(N + 1)^2$ laser sources combined with SLMs on a spherical or hemispherical surface around the observer as represented in Fig. 4.2, each source regenerating a piece of the object that lies in a tile of the spherical surface around the object hologram, however further processing is for sure necessary.

The second approach to decoding is angle-based decoding, which can be fed into the implemented algorithm for LFD displaying of holograms, namely Hol2LFD. This method is expected to work analogously to publicly available holographic image datasets that contain multi-view holographic image data such as BCOM [61]. This dataset contains

high-resolution 2D holographic data, which with the help of NRSH can be rendered as if it is seen from different angles. The resulting rendered images constitute this hologram seen from different angles which then can be processed into quilt format to be displayed through LFD.

Here the implemented algorithm supplies an automated workflow of taking holographic image data from publicly available datasets as input, processing them from different angles by utilizing NRSH, and creating quilt images to make them suitable to be displayed on LFD. The process is controllable through a GUI. This algorithm here and after is called Hol2LFD.

The source codes of version 1.0 of the project are publicly shared and maintained on GitLab of the faculty at the address <https://gitlab.fel.cvut.cz/ozdogard/Hol2LFD>. The work on the code will be continued on the address.

4.2 Encoding of object wavefields based on SHT

In this section, encoding the object wavefield by SHT is described theoretically. Firstly, the reasoning behind why SHT is selected as an encoding method is given, and after that, a theoretical explanation is done. A block diagram of SHT encoding is given in Fig. 4.3 for easier understanding. Fig. 4.3 expands the encoding and decoding using inverse SHT parts shown in Fig. 4.1 (all the turquoise blocks on the left side of the diagram).

The theory explained in sections 4.2.2 and 4.2.3 are summarized from [30], in order to make the mathematical perspective of SHT encoding clearer. This note here is given in order to avoid overusing citations. The citations are included in the section headings.

4.2.1 Reasoning of selection of the encoding method

Both sound and light fields have some similarities. Even though the light is an electromagnetic wave and sound is a mechanical wave with completely different wavelengths granting different physical properties, both types of waves propagating through space share a similar wave nature. Some of the similarities between sound and light fields include:

1. **Wave nature:** Both sound and light fields are wave-like in nature and can be described by their frequency, wavelength, and phase.
2. **Propagation:** Both sound and light fields propagate through space, and their behavior can be described by the wave equation.
3. **Interference:** Both sound and light fields can interfere with one another, resulting in constructive or destructive interference patterns that can be observed in the pressure or intensity patterns.
4. **Diffraction:** Both sound and light fields can diffract around objects, resulting in the spreading and bending of the wavefronts.

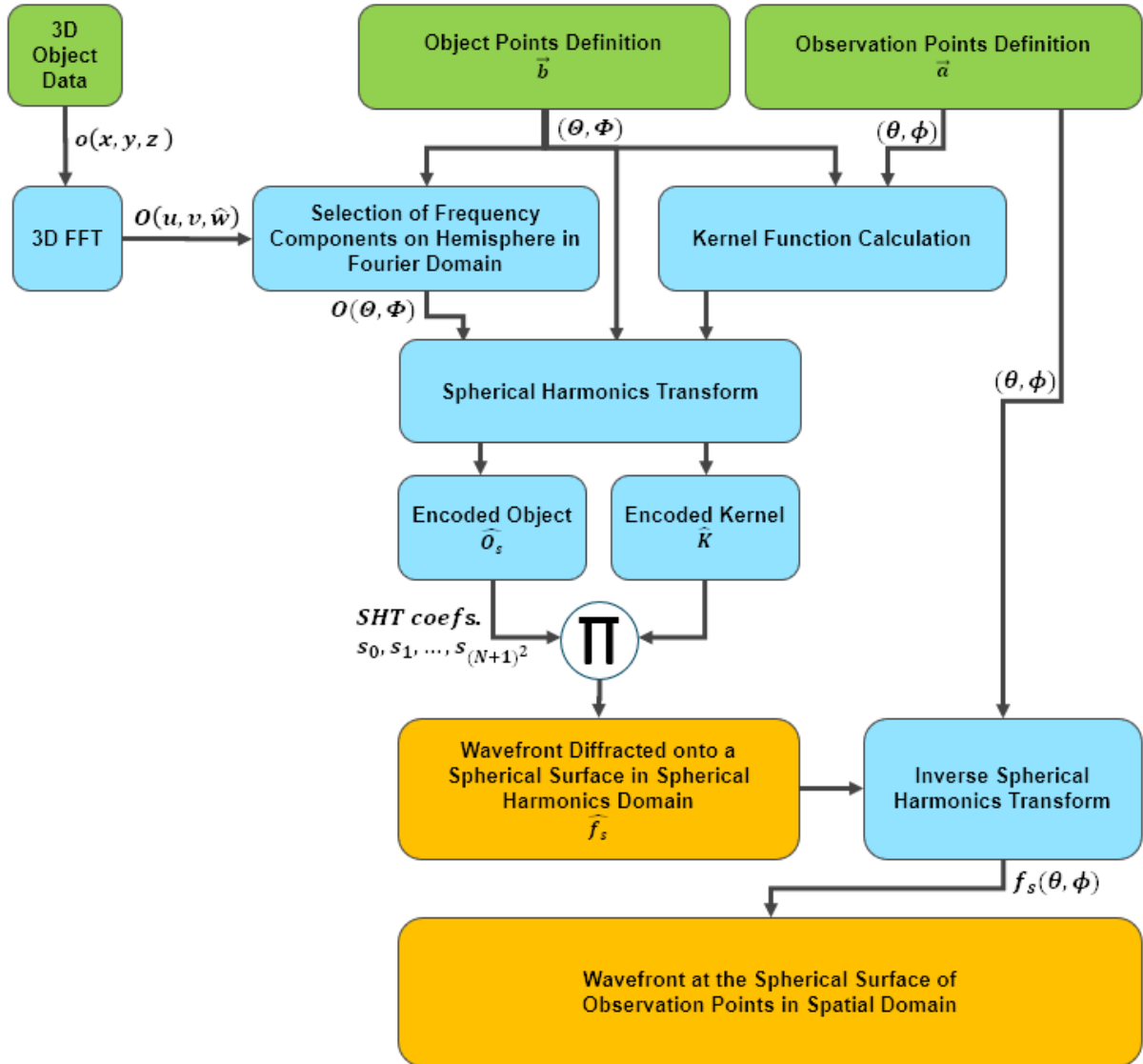


Figure 4.3: SHT encoding block diagram.

5. **Scattering:** Both sound and light fields can scatter when they encounter obstacles, leading to a change in the direction and intensity of the wave.
6. **Wavefront shaping:** By the utilization of interference the light wavefronts and pressure field wavefronts can be manipulated and this property eventually can be used to construct complex light and sound fields at a distance.

These similarities between sound and light fields arise from the fact that both types of waves can be described by similar mathematical models, such as the wave equation and

Maxwell's equations. They can be understood using similar physical principles, such as the principles of wave optics and acoustics.

When the Helmholtz Equations describing light wave and sound wave propagation are compared (respectively Eq. 2.23 and Eq. 2.42), the differentiating part is in the propagation vectors

$$k_l = \frac{w_l}{c_l}, \quad k_s = \frac{w_s}{c_s} \quad (4.1)$$

where k_l, k_s are the light and sound propagation vectors, respectively, w_l, w_s are the light and sound angular frequencies and c_l, c_s are the light and sound speeds in a medium.

Given the fact that SHT is theoretically and physically applied in sound systems [37] and in computer graphics [26], especially in illumination and its manipulation through the scenes, SHT is a perfect candidate for 360-degrees hologram encoding. Moreover, theoretical applications as presented in [28, 30], SHT shows excellent potential in the area by overcoming the viewing angle dependencies of cylindrical holograms [29, 38]. Therefore, a spherical hologram is considered ideal for realizing the whole viewing zone and for reconstructing a large object in both the horizontal and vertical directions [30].

4.2.2 Wavefront on the spherical surface

In CGH, in order to encode a hologram, the wavefront diffracted from that object should be recorded. For a spherical hologram encoded by SHT, the wavefront on a spherical surface (in spherical coordinates) diffracted from a 3D object defined in cartesian coordinates should be encoded. Therefore, the planar wavefront $f_p(x_p, y_p)$ diffracted from an object $o(x, y, z)$ to a planar surface at distance R in the z direction, is given by

$$f_p(x_p, y_p) = \frac{i}{4\pi} \int \int \frac{O(u, v, w^s)}{w^s} \exp(i2\pi R w^s) \times \exp[i2\pi(ux_p + vy_p)] dudv, \quad (4.2)$$

where $O(u, v, w)$ is the 3D Fast Fourier Transform (3D FFT) components of the object and $\exp(i2\pi R w)$ is the phase propagation. The component w^s will be explained shortly. In order to represent 3-dimensional FFT coefficients in 2-dimension in the spherical coordinates on a constant radius spherical surface, a conversion from spatial frequencies (u, v, w) has to be done to (Θ, Φ) . This conversion enables indexing the coefficients of $O(u, v, w)$ laying on a hemispherical surface of radius $1/\lambda$ as $O_s(\Theta, \Phi)$. An illustration is given in Figure 4.4. For this indexing operation, the following transformations are used,

$$u = \left\lfloor \frac{1}{\lambda} \sin\Theta \cos\Phi \right\rfloor, \quad (4.3)$$

$$v = \left\lfloor \frac{1}{\lambda} \sin\Theta \sin\Phi \right\rfloor, \quad (4.4)$$

$$w^s = \left\lfloor \sqrt{\frac{1}{\lambda^2} - u^2 - v^2} \right\rfloor \quad (4.5)$$

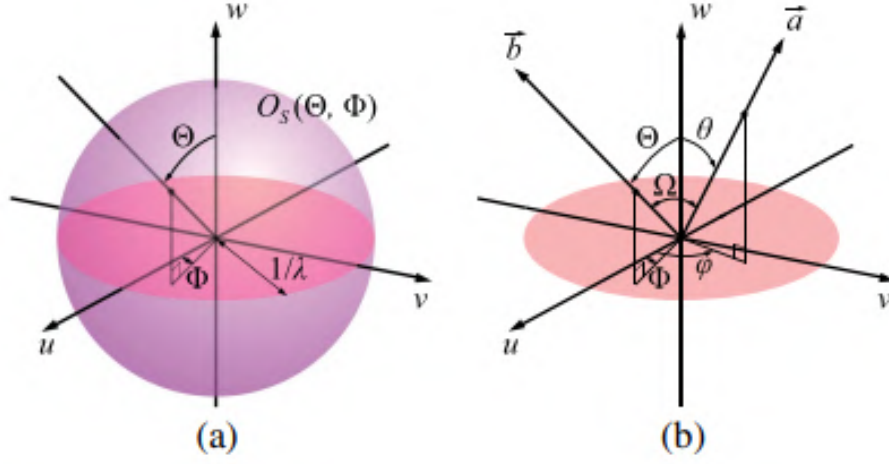


Figure 4.4: (a) Selection of components on the hemispherical surface of radius $1/\lambda$, (b) observation vector a and Fourier component points vector b where (u, v, w) is practically equivalent to cartesian coordinates (x, y, z) in spatial frequency domain. Ω represents the angle between vectors \vec{a} and \vec{b} (taken from [30]).

where $\lfloor x \rfloor$ is the floor sign. Given Eq. 4.2, the wavefront at $(x_p, y_p) = (0, 0)$ is

$$f_p(0, 0) = \frac{i}{4\pi} \int \int \frac{O(u, v, w^s)}{w^s} \exp(i2\pi R w^s) \times dudv \quad (4.6)$$

When variables (Θ, Φ) are introduced instead of (u, v) , the $f_s(\theta = 0, \phi = 0)$ is equal to $f_p(x_p = 0, y_p = 0)$

$$f_s(0, 0) = f_p(0, 0) = \frac{i}{4\pi\lambda} \int_0^{2\pi} \int_0^\pi O_s(\Theta, \Phi) \exp\left(\frac{i2\pi R \cos\Omega}{\lambda}\right) \sin\Theta d\Theta d\Phi, \quad (4.7)$$

$$= \frac{i}{4\pi\lambda} \int \int_S O_s(\Theta, \Phi) K(\cos\Omega) ds \quad (4.8)$$

where $f_s(\theta = 0, \phi = 0)$ is the wavefront on the spherical surface at the observation point $(\theta = 0, \phi = 0)$ and K is the Kernel function representing the phase propagation. Hence, Kernel function K and infinitesimal area on the sphere ds can be written as,

$$K(\cos\Omega) = \text{rect} \left[\frac{\Omega}{\pi} \right] \exp\left(\frac{i2\pi R \cos\Omega}{\lambda}\right) \quad (4.9)$$

$$ds = \sin\Theta d\Theta d\Phi \quad (4.10)$$

The function $\text{rect}[x] = 1$ if $x < 1/2$, otherwise 0. This function extends the integration over the positive hemisphere to the whole sphere, note that the Θ integration limits on Eq.

4.7. $\cos\Omega$ is the relative angle between (inner product of) the vectors a and b as shown in Figure 4.4. This formula can be generalized over the whole spherical surface as follows,

$$f_s(\theta, \phi) = \frac{i}{4\pi\lambda} \int_0^{2\pi} \int_0^{\pi/2} O_s(\Theta, \Phi) K(\cos\Theta) \sin\Theta d\Theta d\Phi \quad (4.11)$$

$$K(\cos\Theta) = \text{rect} \left[\frac{\Theta}{\pi} \right] \exp\left(\frac{i2\pi R \cos\Theta}{\lambda}\right) \quad (4.12)$$

$$ds = \sin\Theta d\Theta d\Phi \quad (4.13)$$

In Eq. 4.11, O_s doesn't contain any directional propagation information, it is just indexed Fourier coefficients, on the other hand, $K(\cos\Omega)$ includes the propagation and the contribution of the coefficients to a propagation direction which is results of $\cos\Omega$ term. Note that Ω is a function of $\Theta, \Phi, \theta, \phi$.

Eq. 4.11 can be notationally simplified as,

$$f_s(\vec{a}) = \frac{i}{4\pi\lambda} \int \int_S O_s(\vec{b}) K(\vec{a} \cdot \vec{b}) ds \quad (4.14)$$

where \vec{a} is the direction vector to the spherical observation surface and \vec{b} is the Fourier components vector of the object, as shown in 4.4. This equation can be interpreted as the convolution integral on the sphere [39]. The simplified computation of this integral can be achieved by utilizing SHT because $K(\vec{a} \cdot \vec{b})$ is symmetric with respect to \vec{a} , [40, 62], and the convolution theorem on a spherical surface is as follows,

$$\hat{f}_s^m = C \hat{O}_s^m \cdot \hat{K}^m \quad (4.15)$$

where \hat{f}_s^m , \hat{O}_s^m and \hat{K}^m are SHT coefficients of order m of f_s , O_s and K and C is a constant.

Eq. 4.15 can be simply explained as:

SHT is a transform that analyzes the spatial distribution of a function on a spherical surface, simply said a spherical FFT. Hence, just like the convolution in the time/spatial domain is equivalent to a multiplication in the frequency domain for FFT, convolution in the spatial domain is equivalent to a multiplication in the SHT domain. Hence Eq. 4.14 can be simply computed in SHT domain as Eq. 4.15.

4.2.3 Sampling pitch

The sampling pitch required to be able to perform SHT of O_s and K should be calculated. The correct selection of SHT will prevent aliasing errors during the processing of the signals. Since the SHT is taken on a spherical surface with a constant radius the sampling pitch depends on the position or the surface arc that is being processed, hence it is calculated differently for Fourier components of the object (O_s) and the Kernel function K . This calculation is similar to that of 2D FFT.

Given that zenithal and azimuthal sampling are notated by $\delta\Theta$ and $\delta\Phi$ respectively, the arcs on the spherical 3D FFT surface become $\delta\Theta/\lambda$ and $\delta\Phi/\lambda$ respectively. If the diagonal length (longest length) of the object is represented as D , the sampling pitch becomes,

$$\delta\Theta = \frac{\lambda}{D}, \quad \delta\Phi = \frac{\lambda}{D\sin\Theta} \quad (4.16)$$

Notice that $\delta\Phi$ is dependent on Θ because azimuthal length depends on the zenithal angle.

Following a similar approach, the sampling pitch for the Kernel function can be calculated as,

$$\delta\Theta = \frac{\lambda}{R} \quad (4.17)$$

Notice that since the arc being sampled lies on the observation surface the divider is R .

4.2.4 Practical trial of SHT encoding

The encoding method published in [30] is tried to be recreated. Even though, the encoding and decoding of 2D Fourier coefficients $O_s(\Theta, \Phi)$ by SHT (hence \hat{O}_s) are achieved, the multiplication by encoded Kernel function \hat{K} has made the wavefront not suitable for reconstruction. In the trials, the encoding and decoding of O_s to and from \hat{O}_s is achieved without any trouble as shown in Fig. 4.5, however the multiplication with encoded \hat{K} disrupts the reconstruction of the object and disables the hologram creation. The missing or unrepresented middle stages in the paper [30] carry crucial importance in the recreation of the method.

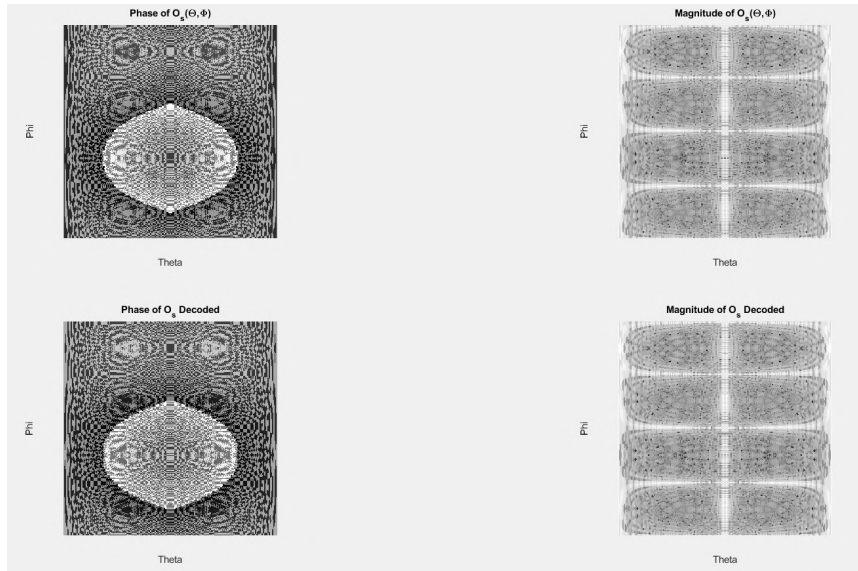


Figure 4.5: Encoded and decoded O_s

Another aspect, which is also mentioned in the [30], is that the memory requirement of the theoretical approach is demanding because of the required sampling pitch. Hence the experiments are conducted in very large wavelengths compared to visible light. Moreover, because of the time and equipment limitations, these trials are left to be continued in a future time.

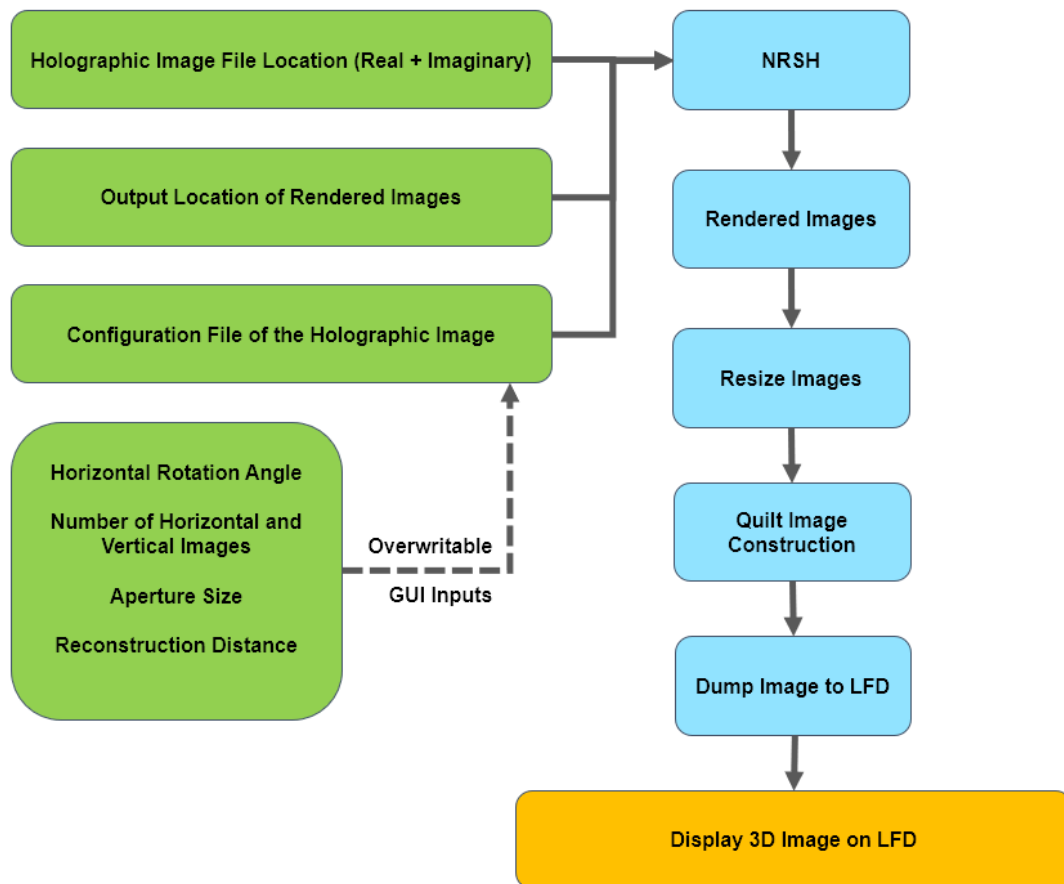


Figure 4.6: Block diagram of the displaying method. The external inputs to the system are given in green color, the intermediate steps are given in turquoise color, and the outputs of the system are given in orange color. The whole system constitutes the Hol2LFD.

4.3 Displaying of holographic images on LFD

As described before LFDs establish a great tool for visualizing 3D objects and holograms. So the experimental approach here is based on demonstrating 3D multi-view holograms on Looking Glass Portrait (LGP) by processing holographic image data contained in JPEG Pleno Database under Holography Datasets. The main goal here is to create a workflow

and working software to process and render 2D holographic images from certain angles, prepare them in a suitable format to be displayed in LGP, and display them in possessed LGP.

The proposed software Hol2LFD tries to enable the LFD displayable image creation in a user-friendly way by utilizing NRSH and publicly available holographic image datasets. The pipeline of **Hol2LFD** is given in Fig. 4.6. This pipeline describes the yellow block in Fig. 4.1 in detail.

Hol2LFD has a GUI where the user can input the holographic image data consisting of two high-definition images, real and imaginary parts of the holographic image, and a configuration file that enables the user to render the holographic image from different perspectives. Even though the system contains preset configuration files, some inputs can be overwritten by the user, these will be explained later. Supplying these inputs to NRSH will render the images and save each perspective in a folder. Later these perspectives are read by Hol2LFD to create a quilt image format that the LFD can interpret and display as 3D. Finally, these images are flashed into the available LGP.

4.3.1 Input Selection and Limitations

Together with the NRSH software, there are already some configuration files present. However, these files contain general information about the holographic image reconstruction method such as: wavelength, pixel pitch, and the reconstruction/propagation method of the hologram. These parameters are mostly related to the recording of the hologram. However, other aspects that are contained in the configuration files are independent reconstruction parameters. The ones that are related to the LFD and to the Hol2LFD are explained below.

Inputs

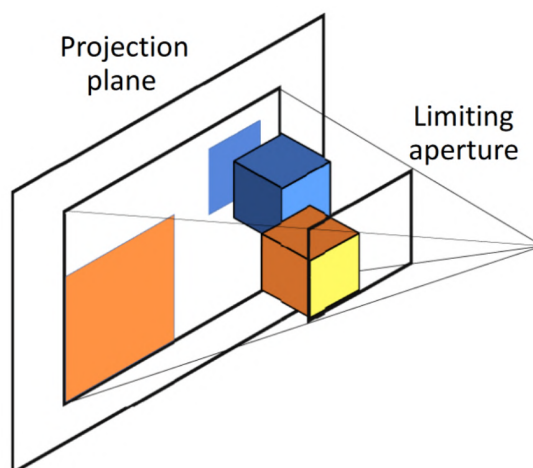


Figure 4.7: Synthetic aperture illustration (taken from [61]).

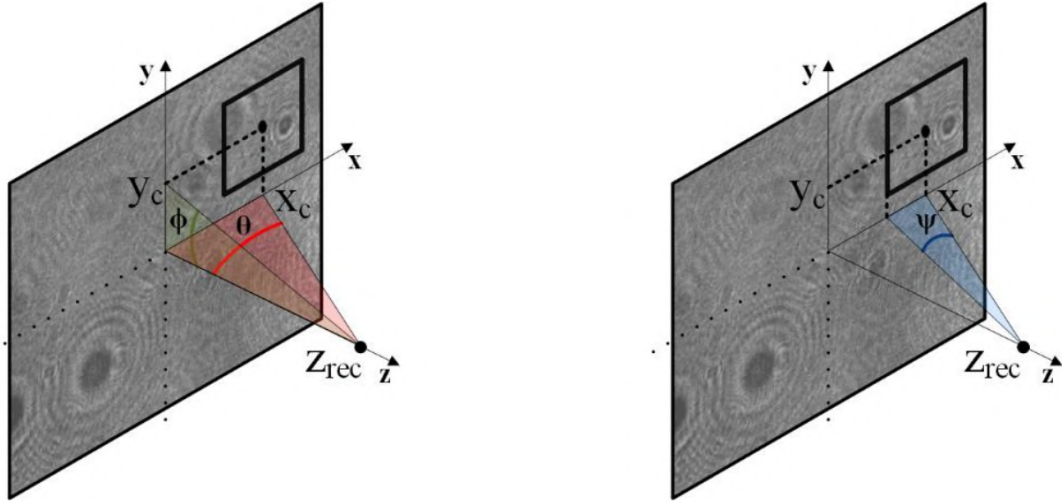


Figure 4.8: Synthetic aperture on Fourier components determines which parts will be propagated. Here θ , on the left, represents the horizontal rotation angle, and ψ , on the right, represents the aperture size (taken from [74]).

- **Horizontal rotation angle:** This input will change how many degrees the perspective will rotate. The given input here will shift the synthetic aperture in the horizontal direction, see Fig. 4.8.
- **Number of horizontal and vertical images:** Defines the quilt image aspect ratio, the suggested ratio is 4:3 (V:H), which aligns with the aspect ratio of the LFD. It also defines the total number of perspectives.
- **Aperture size:** The aperture size in degrees can be considered as the hole that the light will shine on the objects, a good illustration is shown in Fig. 4.7, the proper selection of the aperture size will change the sharpness of the image.
- **Reconstruction distance:** Reconstruction distance will determine where the focus in terms of the object depth will be placed.

The relation between horizontal rotation angle and aperture can be further explained as follows. Two angles are used to determine the aperture position in the hologram plane shown in 4.8: the horizontal angle,

$$\theta = \arctan(X_c/Z_{rec}) \quad (4.18)$$

and vertical angle,

$$\phi = \arctan(Y_c/Z_{rec}) \quad (4.19)$$

Considering these equations the aperture angle ψ should be set properly so that the square aperture lies inside the hologram plane bounds [74].

The careful selection of the input parameters plays a crucial factor in the proper rendering of the perspectives, hence the quality of the observed image on LFD. The limiting factors and causes are given as follows.

Limitations

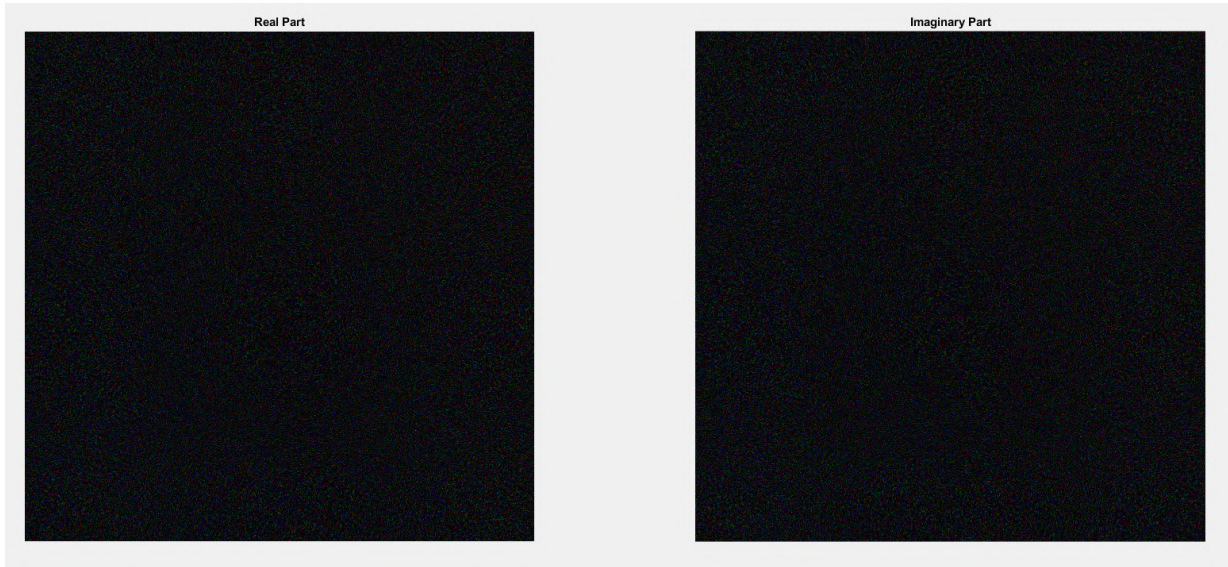


Figure 4.9: Holographic image data that is contained in dices4k holographic image in BCOM dataset. On the left real part of the hologram and on the right imaginary part of the hologram is represented. The reconstructed version of this image is in Fig. 4.11

- **Horizontal rotation angle:** It is not possible to rotate an image limitlessly, however, this limit depends on many parameters, but mostly reconstruction distance and aperture size. Rotating the image in positive angles means shifting the aperture seen in 4.8 to the right and vice versa. If the reconstruction distance is short and the holographic image data has enough resolution (size in x,y) it is possible to rotate the to -10 to -20 degrees, however, if the reconstruction distance is long even a slight rotation will take the aperture out-of-bounds hence no rendering.
- **Number of horizontal and vertical images:** The main limitation here is caused by LFD. Because for a rotation angle of 20 degrees for a total of 20 images will cause discrete steps in the horizontal view of the LFD image. However, 121 images in a quilt image make the LFD image blurry during observation. The most commonly applicable value has been found to be 48 total images containing 8 horizontal to 6 vertical images.

4. A METHOD TO ENCODE AND DISPLAY HOLOGRAMS

- **Aperture size:** The aperture size determines the sharpness however, too big of an aperture size will make the image blurry and depending on the reconstruction distance will be out of bounds (if the reconstruction distance is too big). For practical applications, it was seen that between 5 - 8 degrees are useful.
- **Reconstruction distance:** This parameter will mainly affect the out parameter limitations. During NRSH usage without any rotation, it will synthesize the images even if the focus is out of the bounds of the scene, however, will not be visible, distinguishable, or understandable. This reconstruction distance heavily depends on the selected holographic image, each dataset contains a range of reconstruction distances for all the included images.

4.3.2 An example of conversion using Hol2LFD

In this section an example reconstruction is explained with figures showing the main steps of the reconstruction, starting from the holographic image data to the last screen of the software which is then sent to LGP.

Holographic image data of dices4k of BCOM dataset is shown in Fig. 4.9 ¹.

Inputs			
-Input Files-			
C:/Users/asus/Desktop/THESIS/LFD/LGP/Hol2LFD/jpeg-pleno-nrsh/hologram_images/dices4k-RI/dices4k_real.exr		Select the Real File	
C:/Users/asus/Desktop/THESIS/LFD/LGP/Hol2LFD/jpeg-pleno-nrsh/hologram_images/dices4k-RI/dices4k_imag.exr		Select the Imaginary File	
C:/Users/asus/Desktop/THESIS/LFD/LGP/Hol2LFD/jpeg-pleno-nrsh/config_files/bcom/dices4k_000.txt		Select the Config File	
-Select the angles-			
Vertical Angle:	0	-	0
Horizontal Angle:	-20	-	20
-Select number of rows and columns-			
No of Vertical Images:	6	No of Horizontal Images:	8
-Reconstruction Distance or Distances-			
Reconstruction distance:	0.0017	Aperture Size:	6
-Choose the output File-			
C:/Users/asus/Desktop/THESIS/LFD/LGP/Hol2LFD/figures		Select Folder	
dices4k_000			
Back	Hol 2 PNG	Log Page	Quit

Figure 4.10: Input page of Hol2LFD, the necessary input parameters are entered for dices4k quilt image construction.

When the program is run and Hol2LFD tab is selected, in input page comes up. The necessary parameters are filled up, as shown in Fig. 4.10, for the holographic image to

¹For possible printing issues: the two images contain red, green, and blue speckles with no sign of any silhouettes of any dice, rendered version is in Fig. 4.11.

be rendered by NRSB software. The inputs contain real and imaginary image files, configuration file, minimum and maximum horizontal rotation angles, number of vertical and horizontal images, reconstruction distance in meters, aperture size in angles, and output destination.

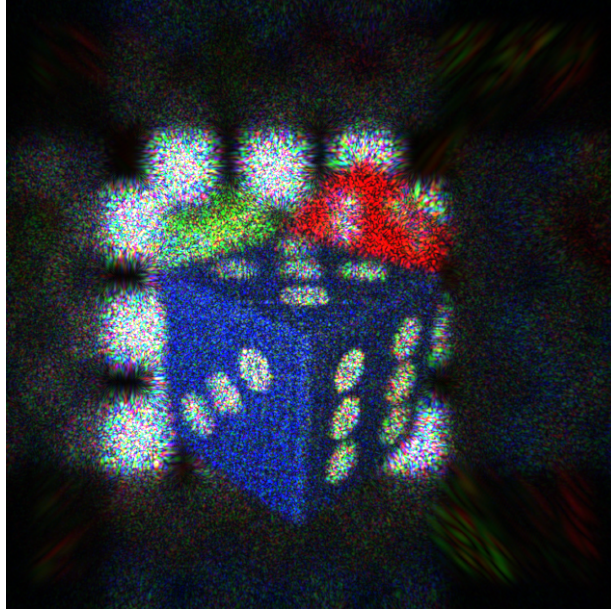


Figure 4.11: Single rendering (propagation by NRSB) of dices4k of BCOM dataset, with reconstruction parameters: -7.23404 degrees horizontal rotation, 6 degrees aperture size, and 0.0017 meters of reconstruction distance.

Please note that there are also minimum and maximum vertical rotation angles in the inputs. Even though LFP doesn't support the demonstration of vertical rotation, NRSB software does. Equal selection of these parameters will render images from only that angle, and any angle that the NRSB is capable of generating will be accepted. However, the reason for keeping the range is for experimental trials and for future development of the method. When a range is entered, the observed hologram on LFP rotates diagonally when the observation angle moved horizontally. However, the image becomes blurry and not really stable.

One of the resulting images is demonstrated in Fig 4.11. These single images are saved separately. The total amount of images are

$$N_t = N_h \times N_v \quad (4.20)$$

where N_h and N_v are the numbers of horizontal and vertical images, respectively. Hence the resulting horizontal rotation angle array becomes:

$$\theta_{arr} = \text{linspace}(\theta_{min}, \theta_{max}, N_t) \quad (4.21)$$

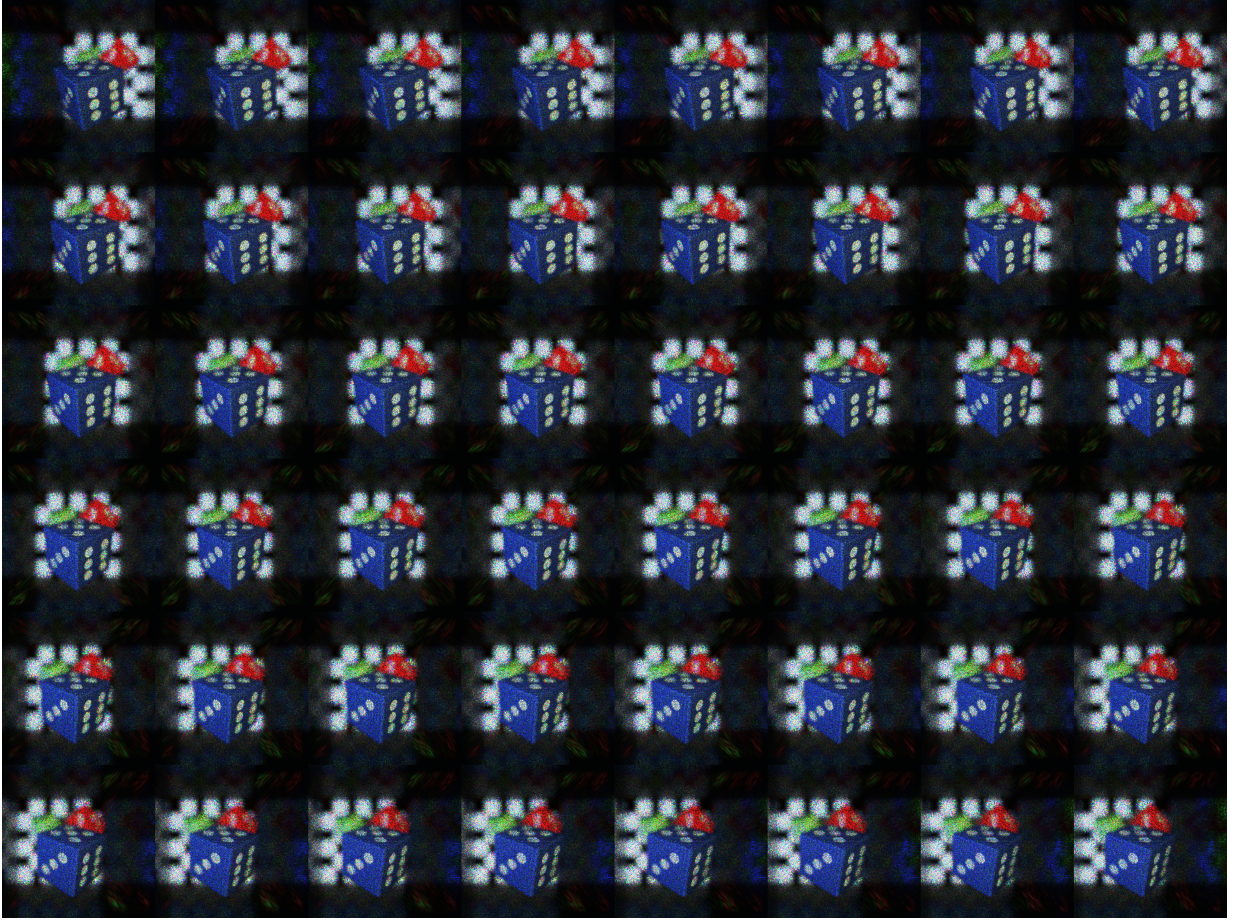


Figure 4.12: Quilt image ready to be sent to LFD that was reconstructed with input parameters to Hol2LFD: -20 to 20 degrees horizontal rotation, 6 vertical and 8 horizontal images, 6 degrees aperture size, and 0.0017 meters of reconstruction distance.

where $\text{linspace}(x, y, z)$ function divides the range of $[x, y]$ into total of z equidistant points. $\theta_{min}, \theta_{max}$ represents the minimum and maximum horizontal rotation.

After all the images are rendered for every angle, an image processing algorithm reads all the images resizes them properly, and creates the quilt image. In order to save memory but still create a sufficient quality (if and for future processing) the quilt image is currently set to be:

$$\text{Height} = 6 \times 1024px, \quad \text{Width} = 8 \times 1024px \quad (4.22)$$

This number is selected in accordance with the aspect ratio of the LGP and the image itself. The quilt image is shown in Fig. 4.12.

The image is again resized and demonstrated in the Hol2LFD, and then sent to LGP¹. In Fig. 4.13, pictures of the displayed image from different angles on the setup are shown.

¹For online readers there is a video added to the gitLab repo that demonstrates the hologram on the



Figure 4.13: LFP displaying processed dices4k of BCOM dataset from 3 different angles.

LFP. Note continuum: The initially uploaded video might contain jumps between observation angles this transition is smoother in real-life. This problem will be fixed and the video will be updated in gitLab repo.

Conclusions

In this section, the achieved work is summarized emphasizing the main focus points, contributions are highlighted, possible future work and shaped ideas are described, and the study is concluded.

5.1 Summary

Holography has been developing theoretically since the early 1900's, [1], however, the advancement of computational power enabled computer-generated holography (CGH) and digital holography to be studied and experimented with. Hence, unconventional methods started to arise, creating a deeper understanding of holography and enabling cutting-edge processing and displaying methods. Proper implementations CGH would enable the development of possible applications and commercial products in fields such as 3D displays, security, virtual/augmented reality, education, and entertainment. Despite the advances in CGH, image acquisition, processing, and reproduction still face challenges such as noise interference, computational intensity, and quality degradation during reconstruction. This paper tries to address holographic encoding and reproduction by reviewing current CGH technology and tries to scratch the surface of the complicated world of holography.

Two different areas are brought into focus. The first is on a comprehensive state-of-the-art encoding approach to spherical computer-generated holography (SCGH), and the second is the display method especially focused on displaying holographic images on light field displays (LFDs). The main reason for the selection of SCGH is that as the practical applications of spherical harmonics transform (SHT) became more spherical harmonics are understood better and started to be applied in holography as well. In the literature, it is suggested that SCGH eliminates the viewing angle limitations. Just as the cylindrical CGH overcomes the horizontal view angle limitation of planar CGH, SCGH overcomes the vertical view angle limitation, hence achieving a full sphere view angle. The main reason for the selection of the LFDs is the practicality of the implementation and experimental testing. Widely and commercially available LFDs enable the construction of functional software that can be tested, demonstrated, and evaluated in the physical world.

After the explanation of the fundamentals of light and holography, spherical harmonics are explained to set the foundation for the SHT used in investigated SCGH method. Current methods for CGH and display technologies are reviewed. In this work, the encoding of 360-degree CGH using spherical harmonics, proposed in [30] is investigated and tried to be recreated, and a new software connecting holographic image conversion and its display on LFD is presented. Moreover, an idea of a workflow, starting from the object wavefield encoding to the reproduction method, is drafted and described.

The theoretical starting point was to be able to set up a workflow to enable the encoding, manipulation, and reproduction of objects. A workflow idea is established and the steps can be briefly explained as follows. The object in cartesian coordinates diffracts an object wavefield on a spherical surface around the object. Since SHT is able to describe complex functions on a spherical surface efficiently with only a few coefficients, efficient encoding of this wavefield using SHT can also enable full construction of the full object. Encoded wavefields can easily be manipulated using spherical harmonics rotation, warping, or filtering matrices, which are implemented functions in many publicly available SHT tools. For the decoding and displaying of this encoded field two different approaches are presented, one of which is hypothetical and the other practical. The hypothetical approach is somewhat analogous to the higher order ambisonics reproduction method. The decoded signals will construct $(N + 1)^2$ channels which then can be fed into an equal amount of laser sources equipped with transmissive spatial light modulators positioned around the sphere or hemisphere. With further processing of these channels, the sources can create either a tile of the object or contribute to the whole object. This approach would be especially useful for large-scale applications such as concerts, audiovisual exhibitions, etc. However, the computational, theoretical, and practical aspects are out of the scope of this work.

The practical approach consists of displaying these objects in a limited manner through LFDs. This can be done by decoding the object, rendering it for certain angles, and creating a quilt image to be fed into the LFD. Since the whole object field is encoded and can be manipulated, it is easily renderable for necessary angles. The good part of the practical object is that it enables the usage of publicly available holographic image datasets. These holographic images can be rendered for limited angles and a quilt image can be constructed. Finally, constructed quilt images can be displayed using LFD.

The experimental standpoint can be explained in two different parts, encoding of holographic objects using SHT and displaying of holographic images. Firstly, SHT encoding is taken into account. During the investigation of the possible SCGH models, the encoding method based on SHT proposed in [30] seemed promising. Hence started to be implemented. Based on the reference paper, the Fourier components of the object that lie in the hemisphere with a radius of $1/\lambda$ in the Fourier domain are indexed to achieve the spherical representation of the 3D FFT. Encoding and decoding of these components using SHT are achieved. Directional propagation information containing Kernel functions are calculated based on the observation direction in the spherical domain, and encoded. In order to achieve the convolution integral these encoded parts are simply multiplied as stated in [30] and the supposed wavefield diffracted onto the spherical surface at the observation distance should have been achieved. However, during the decoding of this

wavefront at reconstruction angles, the holograms haven't been able to be reconstructed. Hence, the feasibility of the system couldn't be demonstrated. Secondly, the displaying of holographic images is taken into account. Here, one of the most determining criteria was the availability of an LFD, commercially named Looking Glass Portrait (LGP). Physical accessibility of this device enabled building software that is eventually capable of displaying holographic data, which is either decoded from SCGH or taken from publicly available datasets such as BCOM. Since the decoding is not achieved, the holographic image data is taken from these datasets. The proposed software Hol2LFD is capable of reading these high-resolution Multiview-plus-Depth containing images, running state-of-the-art numerical reconstruction software for holography (NRSH) to render the holographic images from different perspectives, creating quilt images (LGP images) and flashing these images to LGP. The software also contains a GUI where some of the reconstruction parameters can be inputted changing the preset configurations that are prepared during the experiments. These parameters contain the most important parameters for the rendering of an LGP image. These are horizontal rotation angle, reconstruction distance, aperture size, and the number of vertical and horizontal images. The first three parameters are dependent on the holographic images and the selection of these parameters affects the rendering performance of the NRSH. The optimum values of these parameters are highly dependent. The latter two affect the observation of the displayed image on the LGP, when the total number is set too low displayed image seems to have distinct jumps for different angles of observation, when set too high the displayed image becomes too blurry and diffused. Values that are tested and seen to be working with a decent performance have been preset into the configuration files.

To conclude, this work tried to analyze unconventional techniques for computational holography. Here, a possible workflow for CGH consisting of state-of-the-art methods is presented. An encoding method is tried to be incorporated, however, it was not successfully accomplished. As a milestone, an initial version of a working software that is capable of converting publicly available holographic images in maintained repositories is presented and publicly published.

5.2 Contributions of the master's thesis

The main contributions are briefly listed here.

- A review of the latest trends in CGH and holographic display technologies is made.
- A workflow for CGH minding the state-of-the-art encoding and displaying of the holographic data is proposed.
- A software that is capable of converting holographic images to LFD-suitable images is constructed and publicly published.
- Preset configuration files conversion of some of the publicly available holographic images are prepared.

5.3 Future work

Based on the achieved work, analyzed literature, and gained knowledge, the extension of this thesis seems possible in the below-listed areas.

- **Framework construction:** From a conceptual point of view, the workflow seems theoretically possible with the current state of the technology, however from a practical perspective, it is important to investigate the workflow deeper and make it into a framework.
- **Perfecting the encoding method:** Despite the extensive exploration of SCGH, the encoding method analyzed was not successfully implemented. There is a need for further research to fully understand and implement the reconstruction of the object, and check the viability and quality of the encoding method. If these are successfully done, the possibility of tiling for larger-scale reconstructions and systems
- **Maintaining and updating the software:** Making the software compatible with all operating systems and LFDs, and maintaining is a challenging yet achievable task. API working together with JPEG Pleno can be created. The GUI can be made more appealing.
- **Extending the preset files and coverage of datasets:** Current holographic dataset coverage is limited. This coverage can be extended to all the datasets contained under JPEG Pleno and preset files can be prepared. Such an endeavor would also improve and externally serve the holography community.

Appendix

Electronic submission contents

Because of the file size limitations, the parts may come in separate zip files and/or some parts may not be included in the zip files. After you unzip the files please arrange them as listed below. The files that are not included in the zip files are mentioned below. These files can be downloaded from the online repo with the address <https://gitlab.fel.cvut.cz/ozdogard/Hol2LFD>.

- **Master's thesis pdf version:** submitted version is compressed hence there might be compression artifacts, uncompressed version is at the repo.
- **SCGH folder:** contains the part of spherical computer generated holography experimental part.
 - **SH_funcs/:** Necessary toolboxes and functions for spherical harmonics transform.
 - **cgh_multip_1.m:** main MATLAB code trying to compute spherical computer generated hologram.
 - **calc_kernel.m** and **calc_kernel_1.m:** different versions of propagation Kernel calculation.
 - **create_obj.m:** object creating function.
 - **createCube.m:** different object creation.
- **Hol2LFD folder:** contains the built software.
 - **~/6x8_figures/:** preconstructed 6x8 all figures. These images are in the repo.
 - **~/11x11_specular_car/:** preconstructed 11x11 specular car. These images are in the repo.

- `~/hologram_images/`: holographic images downloaded from BCOM database. <https://hologram-repository.labs.b-com.com/#/holographic-images>. These images are also included in the repo
 - `~/jpeg_pleno_nrsh/`: NRSH software. <https://gitlab.com/wg1/jpeg-pleno-nrsh>. Please download from the link and include as directed here.
 - `~/reconstruction_configs/`: preset configs for reconstruction.
 - `~/cbor/`: necessary library for writing images to LFD. Add this to your Python PATH or copy this folder to Python scripts.
 - `~/test/`: some test images.
 - `GUI.py`: main code of the proposed application.
 - `hol2lfd.m`: MATLAB function that is called from the Python application.
 - `image_functions.py`: some functions to process rendered images.
 - PNG files: Quilt images ready to be sent to the light field display.
 - `ReadMe.txt`: General information on how to set up and use the program.
- o **JPG files and Video**: the test setup. can be found in the repo.

Bibliography

- [1] D. Gabor, "A new microscopic principle", *Nature*, 161, 777 (1948).
- [2] R.K. Kostuk, "Holography: Principles and Applications", 1st ed., CRC Press, 2019. <https://doi.org/10.1201/9780429185830>
- [3] M. Born and E. Wolf, "Principles of Optics", p. 375, 5th ed., Pergamon Press, Oxford, UK (1975).
- [4] E. Wolf, "Introduction to the Theory of Coherence and Polarization of Light". Cambridge university press, 2007.
- [5] Y. Zhang, L. Dong, Wenjuan Han, Honghao Xu, Junhai Liu, "Spectroscopic properties and microchip laser performance of Yb:LaCa4O(BO3)3 crystal, *Infrared Physics & Technology*", Volume 129, 2023, 104566, ISSN 1350-4495, <https://doi.org/10.1016/j.infrared.2023.104566>
- [6] J. W. Goodman, "Introduction to Fourier Optics", 4th ed., W. H. Freeman, New York (2017).
- [7] P. Lecomte, "Ambitools: Tools for Sound Field Synthesis With Higher Order Ambisonics-V1.0", *Proceedings of the 1st International Faust Conference (IFC-18)*, Jul 2018, Mainz, Germany. <hal-03162948>
- [8] F. Katzberg, M. Maass and A. Mertins, "Spherical Harmonic Representation for Dynamic Sound-Field Measurements," *ICASSP 2021 - 2021 IEEE International Conference on Acoustics, Speech and Signal Processing (ICASSP)*, Toronto, ON, Canada, 2021, pp. 426-430, 10.1109/ICASSP39728.2021.9413708.
- [9] M. Kronlachner, "Spatial transformations for the alteration of ambisonic recordings", 2014, <https://phaidra.kug.ac.at/o:8569>
- [10] M. Poletti, "Unified Description of Ambisonics using Real and Complex Spherical Harmonics", *Proceedings of Ambisonics Symposium*, 2009

- [11] T. Carpentier, "Normalization schemes in Ambisonic: does it matter?", in Audio Engineering Society Convention, 142., 2017, AES
- [12] W. Günther & K. Sven & G. Hartmut & D. Nazif & D. Matthias & T. Stephan. "Liquid crystal display as spatial light modulator for diffractive optical elements and the reconstruction of digital holograms". Proceedings of SPIE - The International Society for Optical Engineering. 4596. (2001) 10.1117/12.447341.
- [13] D. Spangenberg, A. Dudley, P. H. Neethling, E. G. Rohwer, and A. Forbes, "White light wavefront control with a spatial light modulator," *Opt. Express* 22, 13870-13879 (2014)
- [14] D. Pi, J. Liu & Y. Wang, "Review of computer-generated hologram algorithms for color dynamic holographic three-dimensional display", *Light Sci Appl*, 11, 231 (2022). <https://doi.org/10.1038/s41377-022-00916-3>
- [15] C. Guo, S. Liu, and J. T. Sheridan, "Iterative phase retrieval algorithms. I: optimization", *Appl. Opt.* 54, 4698-4708 (2015)
- [16] B.Y. Zel'dovich, et al., "Connection between the wave fronts of the reflected and exciting light in stimulated Mandel'shtam-Brillouin scattering", *JETP lett*, 1972. 15(3): p. 109.
- [17] B. Javidi, "Digital holography: A review," *Optical Engineering*, vol. 41, no. 1, pp. 010801-1-010801-14, 2002.
- [18] M. Z. Mirhosseini, O. S. Magaña-Loaiza, M. Malik, and R. W. Boyd, "Dynamic digital holography," *Advances in Optics and Photonics*, vol. 7, pp. 1-57, 2015.
- [19] T. B. Bahder, "Digital holography and three-dimensional display: Principles and applications", Springer Science & Business Media, 2010.
- [20] V. Petrov, A. Pogoda, V. Sementin, A. Sevryugin, E. Shalymov, D. Venediktov, V. Venediktov, "Advances in Digital Holographic Interferometry", *Journal of Imaging*. 2022; 8(7):196. <https://doi.org/10.3390/jimaging8070196>
- [21] M. Hernández-Montes, F. Mendoza-Santoyo, M. Flores Moreno et al., "Macro to nano specimen measurements using photons and electrons with digital holographic interferometry: a review", *J. Eur. Opt. Soc.-Rapid Publ.* 16, 16 (2020). <https://doi.org/10.1186/s41476-020-00133-8>
- [22] L. Yongjun, H. Keehoon, K. Hwi, K. Hyun-Eui, C. Eun-Young, L. Soohyun, K. Taeone, N. Jeho, C. Hyon-Gon, K. Jinwoong, and H. Joonku, "360-degree tabletop electronic holographic display", *Opt. Express* 24, 24999-25009 (2016)
- [23] H.-G. Choo, T. Kozacki, W. Zaperty, M. Chlipala, Y. Lim, J. Kim, "Fourier digital holography of real scenes for 360° tabletop holographic displays", *Appl. Opt.* 58, G96-G103 (2019)

-
- [24] D. N. Borza, "Specialized techniques in holographic non-destructive testing of composites", *Composites Part B: Engineering*, Volume 29, Issue 4, 1998, Pages 497-504, ISSN 1359-8368, [https://doi.org/10.1016/S1359-8368\(98\)00006-7](https://doi.org/10.1016/S1359-8368(98)00006-7).
- [25] M. Bedrossian, C. Barr, C. A. Lindensmith, K. Nealson, J. L. Nadeau, "Quantifying Microorganisms at Low Concentrations Using Digital Holographic Microscopy (DHM)", *J. Vis. Exp.* (129), (2017) e56343, 10.3791/56343
- [26] M. Alexander, S. Pont, J. Koenderink, "Light field constancy within natural scenes", *Applied optics*, 46, 7308-16, (2007) 10.1364/AO.46.007308.
- [27] R. Yang, J. Wang, C. Chen, Y. Wu, B. Li, Y. Li, N. Chen, B.J. Jackin, "Fast Diffraction Calculation for Spherical Computer-Generated Hologram Using Phase Compensation Method in Visible Range", *Applied Sciences*, 2020, 10(17):5784. <https://doi.org/10.3390/app10175784>
- [28] Y. Sando, D. Barada, B. J. Jackin, T. Yatagai, "Fast calculation of computer-generated spherical hologram by spherical harmonic transform", *Proc. SPIE 10233, Holography: Advances and Modern Trends V*, 102331H (15 May 2017); <https://doi.org/10.1117/12.2264926>
- [29] Y. Li, J. Wang, C. Chen, B. Li, R. Yang, N. Chen, "Occlusion culling for computer-generated cylindrical holograms based on a horizontal optical-path-limit function", *Opt. Express* 28, 18516-18528 (2020)
- [30] Y. Sando, D. Barada, B. J. Jackin, T. Yatagai, "Spherical-harmonic-transform-based fast calculation algorithm for spherical computer-generated hologram considering occlusion culling", *Appl. Opt.* 57, 6781-6787 (2018)
- [31] R. Horisaki, R. Takagi, J. Tanida, "Deep-learning-generated holography", *Appl. Opt.* 57, 3859-3863 (2018)
- [32] H. Goi, K. Komuro, T. Nomura, "Deep-learning-based binary hologram", *Appl. Opt.* 59, 7103-7108 (2020)
- [33] J. Lee, J. Jeong, J. Cho, D. Yoo, B. Lee, B. Lee, "Deep neural network for multi-depth hologram generation and its training strategy", *Opt. Express* 28, 27137-27154 (2020)
- [34] R. Horisaki, Y. Nishizaki, K. Kitaguchi, M. Saito, J. Tanida, "Three-dimensional deeply generated holography", [Invited] *Appl. Opt.* 60, A323-A328 (2021)
- [35] M. H. Eybposh, N. W. Cairra, M. Atisa, P. Chakravarthula, and N. C. Pégard, "DeepCGH: 3D computer-generated holography using deep learning", *Opt. Express* 28, 26636-26650 (2020)

- [36] Shi, L., Li, B., Kim, C. et al., "Towards real-time photorealistic 3D holography with deep neural networks", *Nature* 591, 234–239 (2021). <https://doi.org/10.1038/s41586-020-03152-0>
- [37] M. A. Poletti, "Three-Dimensional Surround Sound Systems Based on Spherical Harmonics", *Journal of Audio Eng. Soc.*, vol. 53/11,1004–1025,2005,<http://www.aes.org/e-lib/browse.cfm?elib=13396>
- [38] T. H. Jeong, "Cylindrical Holography and Some Proposed Applications", *J. Opt. Soc. Am.* 57, 1396-1398 (1967)
- [39] J. R. Driscoll and D. M. Healy, "Computing Fourier transforms and convolutions on the 2-sphere", *Adv. Appl. Math.* 15, 202–250 (1994).
- [40] R. Basri and D. W. Jacobs, "Lambertian reflectance and linear subspaces", *IEEE Trans. Pattern Anal. Mach. Intell.* 25, 218–233 (2003).
- [41] D. Ezra, G. J. Woodgate, B. A. Omar, N. S. Holliman, J. Harrold and L. S. Shapiro, "New autostereoscopic display system", *Stereoscopic Displays and Virtual Reality Systems II*, vol. 2409, pp. 31-40, 1995.
- [42] G. J. Woodgate, D. Ezra, J. Harrold, Nicolas S. Holliman, G. R. Jones and R. R. Moseley, "Autostereoscopic 3D display systems with observer tracking", *Image Communication – Special Issue on 3D Video Technology (EURASIP-1998)*, pp. 131.
- [43] C. van Berkel, D. W. Parker and A. R. Franklin, "Multiview 3D-LCD", *Stereoscopic Displays and Virtual Reality Systems III*, vol. 2653, pp. 32, 1996.
- [44] R. Reichelt, N. Häussler, G. Leister, A. Futterer, & A. Schwerdtner (2008). "Large holographic 3D displays for tomorrow's TV and monitors—Solutions, challenges, and prospects", In *IEEE 2008. LEOS 21st Annual Meeting* (p. 194). IEEE.
- [45] R. Häussler, A. Schwerdtner, N. Leister, "Large holographic displays as an alternative to stereoscopic displays", In *Proc. SPIE* (vol. 6803, p. 68030M), 2008.
- [46] S. Reichelt, H. Sahm, N. Leister, A. Schwerdtner. (2008). "Capabilities of diffractive optical elements for real-time holographic displays", In *Proc. SPIE* (vol. 6912, p. 69120P).
- [47] A. Schwerdtner, R. Häussler, N. Leister, "Large holographic displays for real-time applications", In *Proc. SPIE* (vol. 6912, p. 69120T), (2008).
- [48] N. Leister, A. Schwerdtner, G. Fütterer, S. Buschbeck, J.-C. Olaya, & S. Flon, "Full-color interactive holographic projection system for large 3D scene reconstruction", In *Proc. SPIE* (vol. 6911, p. 69110V), 2008.

-
- [49] Stanley, M., Smith, M. A., Smith, A. P., Watson, P. J., Coomber, S. D., Cameron, C. D., Slinger, C. W., & Wood, A. D. (2004). "3D electronic holography display system using a 100 mega-pixel spatial light modulator", In Proc. SPIE (vol. 5249, p. 297).
- [50] Stanley, M., Conway, P., Coomber, S., Jones, J., Scattergood, D., Slinger, C., Bannister, B., Brown, C., Crossland, W., & Travis, A. (2000). "A novel electro-optic modulator system for the production of dynamic images from giga-pixel computer generated holograms", In Proc. SPIE (vol. 3956, p. 13).
- [51] Slinger, C., Cameron, C., & Stanley, M. (2005). "Computer-generated holography as a generic display technology", Computer, vol. 38, no. 8, pp. 46–53, 2005, IEEE.
- [52] F. Banterle et al., "Advanced High Dynamic Range Imaging: Theory and Practice", CRC Press, 2011.
- [53] F. Pereira and E. A. B. da Silva, "Efficient plenoptic imaging representation: Why do we need it?", 2016 IEEE International Conference on Multimedia and Expo (ICME), Seattle, WA, USA, pp. 1-6, 2016, doi:10.1109/ICME.2016.7552939.
- [54] E. H. Adelson, and J. Y. A. Wang, "Single lens stereo with a plenoptic camera", IEEE Transactions on Pattern Analysis and Machine Intelligence, vol. 14, no. 2, pp. 99-106, 1992.
- [55] R. Ng, "Digital light field photography", PhD thesis, Stanford University, 2006.
- [56] T. Balogh, "The HoloVizio system", in Proceedings of SPIE - The International Society for Optical Engineering, vol. 6055, p. 60550U, 2006.
- [57] G. Wetzstein, D. Lanman, W. Heidrich, and R. Raskar, "Layered 3D: Tomographic image synthesis for attenuation-based light field and high dynamic range displays", ACM Transactions on Graphics (TOG), vol. 30, no. 4, p. 95, 2011.
- [58] Looking Glass Factory. "Looking Glass Portrait - Your Personal Holographic Display." <https://lookingglassfactory.com>, 2023.
- [59] K. Meacham, "Hologram-like Light Field Displays", 2017, URL: <https://contest.techbriefs.com/2017/entries/electronics-sensors-iot/7866>, Accessed: 2023-08-07.
- [60] <https://en.3dimensio.ca/lenticular/>, Accessed: 2023-08-07
- [61] Tobias Birnbaum, Raees K. Muhammad, Cristian Perra, Antonin Gilles, David Blinder, Tomasz Kozacki, and Peter Schelkens, "JPEG Pleno holography presents the numerical reconstruction software for holograms: an excursion in holographic views", Appl. Opt. 62, 2462-2469 (2023)

- [62] R. A. Kennedy, T. A. Lamahewa, and L. Wei, "On azimuthally symmetric 2-sphere convolution", *Digit. Signal Process.* 21, 660–666 (2011).
- [63] T. Ebrahimi, S. Foessel, F. Pereira, P. Schelkens, "JPEG Pleno: Toward an efficient representation of visual reality", *IEEE MultiMedia* 23 (4) (2016)
- [64] JPEG.org, "JPEG Pleno Light Field Dataset", Retrieved from <https://jpeg.org/jpegpleno/>, 2023.
- [65] A. Gilles, P. Gioia, R. Cozot, and L. Morin, "Computer generated hologram from Multiview-plus-Depth data considering specular reflections", in 2016 IEEE International Conference on Multimedia Expo Workshops (ICMEW), 2016, pp. 1-6.
- [66] R. Ziegler, S. Bucheli, L. Ahrenberg, M. Magnor, and M. Gross, "A bidirectional light field - hologram transform", *Computer Graphics Forum*, vol. 26, no. 3, pp. 435–446, doi: 10.1111/j.1467-8659.2007.01066.x. [Online]. Available: <https://onlinelibrary.wiley.com/doi/abs/10.1111/j.1467-8659.2007.01066.x>.
- [67] J. Mäkinen, "From light fields to wavefields: Hologram generation using multiperspective images", Master's thesis, Tampere, 2017. [Online]. Available: <http://URN.fi/URN:NBN:fi:tti-201705261552>.
- [68] A. Zizien, "Plenoptic Imaging and Image Data Conversion", Czech Technical University in Prague, Prague, Czechia, (2019). Retrieved from <http://hdl.handle.net/10467/82899>
- [69] M. Breinig, "Coherence", Knoxville, 2015. [Online]. Available: <http://electron6.phys.utk.edu/optics421/modules/m5/Coherence.htm>.
- [70] A. Gilles, "Fast hologram synthesis methods for realistic 3D visualization", PhD thesis, Rennes, 2016. [Online]. Available: <https://tel.archives-ouvertes.fr/tel-01392677>.
- [71] D. Leseberg and C. Frere, "Computer-generated holograms of 3-d objects composed of tilted planar segments", *Applied Optics*, vol. 27, no. 14, pp. 3020–3024, 1988, issn: 0003-6935. 10.1364/AO.27.003020. [Online]. Available: <https://www.osapublishing.org/abstract.cfm?URI=ao-27-14-3020>.
- [72] A. Asundi and C. Zuo, "Digital holography to light field", in *Proceedings of SPIE*, vol. 9132, 2014, 91320U–1–91320U–8. [Online]. Available: <https://doi.org/10.1117/12.2059775>.
- [73] S. Hamann, L. Shi, O. Solgaard, and G. Wetzstein, "Time-multiplexed light field synthesis via factored Wigner distribution function", *Optics Letters*, vol. 43, no. 3, pp. 599–602, 2018, issn: 0146-9592. [Online]. Available: <https://www.osapublishing.org/abstract.cfm?URI=ol-43-3-599>.

- [74] T. Birnbaum, R. Corda, A. Gilles, R. K. Muhamad, C. Perra, and P. Schelkens, "Numerical Reconstruction Software for Holography (NRSH) User Guide", JPEG Pleno Holography, Version 11.0, 2023.